

Integral equations for flexural-gravity waves: analysis and numerical methods

T. Askham* J.G. Hoskins† P. Nekrasov‡ M. Rachh§

January 3, 2025

Abstract

In this work, we develop a fast and accurate method for the scattering of flexural-gravity waves by a thin plate of varying thickness overlying a fluid of infinite depth. This problem commonly arises in the study of sea ice and ice shelves, which can have complicated heterogeneities that include ridges and rolls. With certain natural assumptions on the thickness, we present an integral equation formulation for solving this class of problems and analyze its mathematical properties. The integral equation is then discretized and solved using a high-order-accurate, FFT-accelerated algorithm. The speed, accuracy, and scalability of this approach are demonstrated through a variety of illustrative examples.

1 Introduction

The motion of a thin plate coupled to a fluid is a subject of longstanding interest in the fields of geophysics and acoustics. In the polar regions, ice sheets floating atop the ocean are often modeled as thin plates that bend and flex in response to hydrodynamic forces. The coupling of plates to acoustic media results in similar wave phenomena and has important implications for aerodynamic stability [60, 39] and sound radiation [37, 52]. In complicated media, these waves exhibit peculiar dynamics that include branching [44, 45], bending [3, 24], and cloaking [53, 85].

In the Arctic, ocean waves interact with sea ice in a dynamic region known as the marginal ice zone. Here, short period waves are attenuated by relatively thin ice, allowing longer periods to travel deeper into the ice pack [78]. The same

*Department of Mathematical Sciences, New Jersey Institute of Technology, Newark, NJ 07102 (askham@njit.edu).

†Department of Statistics and CCAM, University of Chicago, Chicago, IL 60637 (jeremyhoskins@uchicago.edu).

‡Committee on Computational and Applied Mathematics, University of Chicago, Chicago, IL 60637 (pn3@uchicago.edu).

§Center for Computational Mathematics, Flatiron Institute, New York, NY 10010 (mrachh@flatironinstitute.org).

is true in the Southern Ocean, where the opening of sea ice-free corridors allows the sea swell to make contact with Antarctic ice shelves [76, 17]. Meanwhile, tsunami and infragravity waves, largely unattenuated by sea ice, are able to reach the ice shelf to induce significant flexure and calving [13, 15]. While it is difficult to separate the impact of ocean wave forcing from thermodynamic processes, there is growing evidence to support the role of ocean waves in the breakup of Antarctic ice shelves and Arctic sea ice [5, 47, 46, 79]. To weigh these factors, it is critical to understand and model interactions between ice and the ocean at various scales. The problem is inherently multi-scale, since sharp ice features like ridges account for a large portion of the total ice area [41], and can significantly affect wave attenuation and propagation in the polar regions.

In the small thickness limit, the ice-cover can be treated as the boundary of the fluid domain wherein the velocity potential satisfies a fourth order differential equation whose coefficients vary with the thickness of the ice-cover. Extensive work has been done to model the propagation of flexural-gravity waves across various obstructions in ice-covers of uniform thickness. These include narrow cracks [72, 66], wide cracks [22], frozen leads [9], and icebergs [74]; see [71] for a comprehensive overview of these works. In this regime, semi-analytic solutions can be obtained using eigenfunction expansions [33, 68, 30], Carlemann singular integral equations [18], or the Wiener-Hopf method [48, 21, 20, 8]. Interestingly, many of these works find that ice features act as low-pass filters, which may help to explain the attenuation patterns observed in the Arctic.

Less attention has been given to the problem of wave scattering induced by continuous changes in the thickness of the ice, likely because they are more resistant to analytical techniques. Early attempts to solve this problem assume that ice features can be modeled as point inhomogeneities [4, 56] or rely on the shallow-water approximation [57]. In three dimensions, this problem has been approximated using a *ray method* [40], or by using a truncated modal decomposition of the vertical component of the velocity [65]; though for the latter, numerical procedures have only been implemented in two dimensions [10] or for axisymmetric ice floes [11]. An alternate approach is to model the full-thickness of ice which has been used to study wave propagation in crevasses, see [69, 59, 61], for example. However, these continuum models become prohibitively expensive in three dimensions, motivating the design of fast methods that work in the thin-plate regime. Perhaps the most closely related prior method to the present work is [81]. Using Green's identities, the authors construct integral equations for unknowns supported on the water-ice interface to approximate the reflected and transmitted coefficients for incident plane waves in two dimensions.

In this work, we derive a novel integral equation formulation for the fully three-dimensional scattering problem, assuming the thickness is smoothly varying and the region of inhomogeneity is compactly supported. We do this by reducing the problem to an associated boundary integral equation on the ice-covered surface. The reduction occurs in two steps. First, we use standard potential theory techniques to convert the three-dimensional boundary value problem into an integro-differential equation for an unknown defined on the

surface. In the second step, we further reduce this integro-differential equation to an integral equation defined only on the compact support of the perturbation of the thickness. The resulting integral equation is Fredholm second kind and, for a large range of parameters, is provably well-posed. Conveniently, existing numerical methods can be easily adapted to discretize this integral equation with high order accuracy and it is straightforward to establish the convergence of the resulting scheme. Further, the discretized system is amenable to solution by fast algorithms, enabling the scalability of this approach to large scattering problems and (essentially) arbitrary accuracy.

In the solution of the integro-differential equation resulting from the first step of the reduction, one obtains a slowly decaying surface density, a problem that often arises with infinite interfaces. An alternate strategy to the one presented here is the technique of PML-BIE [54], or coordinate complexification [29], which involves complexifying the boundary so that the density decays exponentially and the integration can be performed over a finite region. This method was recently applied in [26] for the solution of two-dimensional water waves with one-dimensional boundary, and we expect that the same can be readily extended to three-dimensions. For this approach, even though the coordinates are complex, high order quadrature schemes [43] and fast algorithms are available. In the present context, the approach adopted here has the advantage of being substantially simpler both to implement and analyze, as well as more amenable to acceleration via traditional fast algorithms. More broadly, integral equation methods of this flavor have been widely applied to scattering problems, and while we do not seek to review them here, we remark that these methods have appeared in several related contexts, including capillary surfers [25, 63], obstacles floating amid surface waves [26], and surface waves on interfaces between insulating materials [7, 6].

The remainder of this paper is as follows. In Section 2, we outline the boundary value problem for flexural-gravity waves, and features of the model. In Section 3, we describe the reduction of the PDE to its associated surface integral equation. Following this, in Section 4 we state key analytical properties of the operators appearing in this integral equation, and in Section 5 we prove existence and uniqueness results. The numerical procedure for solving this integral equation and its convergence are briefly described in Section 6, and we present a number of applications of these methods in Section 7. Finally we discuss the limitations of the present work and areas for future research in Section 8.

2 Problem

Let the fluid domain be defined by the lower half-space $\{(x, y, z) : z \leq 0\}$, and let the ice-covered surface be its top boundary. Then, we have the following

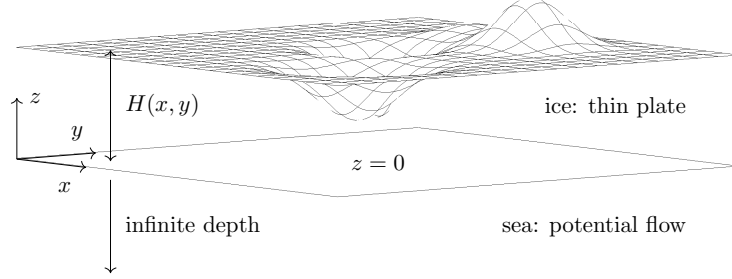


Figure 1: Illustration of the problem setup.

boundary value problem:

$$\Delta\phi + \partial_z^2\phi = 0, \quad z < 0, \quad (2.1)$$

$$(\alpha\Delta_S^2 - \beta)\partial_z\phi + \gamma\phi = 0, \quad z = 0, \quad (2.2)$$

supplemented with suitable decay conditions defined in Section 5. Here, ϕ is the velocity potential, $\Delta := \frac{\partial^2}{\partial x^2} + \frac{\partial^2}{\partial y^2}$ is the surface Laplacian, and Δ_S^2 is the modified biharmonic operator defined below. Though equations like these arise in a number of applications related to acoustics, the setting which motivates the current work is the dynamics of ice-covered oceans. In this context, the coefficients have the following physical connotations: α is the flexural rigidity of the ice, β is the difference in the ice's inertia and gravitational force acting on the fluid, and γ is related to the hydrodynamic pressure:

$$\alpha := \frac{EH^3}{12(1-\nu^2)}, \quad \beta := \rho_{\text{ice}}H\omega^2 - \rho_{\text{sea}}g, \quad \gamma := -\rho_{\text{sea}}\omega^2,$$

where E is the Young's modulus, ν is the Poisson ratio, H is the thickness, ρ_{ice} is the density of ice, ρ_{sea} is the density of ocean water, g is acceleration due to gravity, and ω is the frequency of the hydroelastic wave, which is a fixed parameter of the problem. See Figure 1 for an illustration of the problem setup and Table 1 for common values of these physical parameters. When the flexural rigidity α is allowed to vary in space, the modified biharmonic operator Δ_S^2 acting on the surface $z = 0$ is given by

$$\Delta_S^2 := \frac{1}{\alpha}\Delta(\alpha\Delta) + \frac{1-\nu}{\alpha} \left(2\frac{\partial^2\alpha}{\partial x\partial y}\frac{\partial^2}{\partial x\partial y} - \frac{\partial^2\alpha}{\partial x^2}\frac{\partial^2}{\partial y^2} - \frac{\partial^2\alpha}{\partial y^2}\frac{\partial^2}{\partial x^2} \right).$$

This operator appears in many related works, including [65, 10, 67, 64]. We note that when the flexural rigidity α is constant, this operator simplifies to $\Delta_S^2 = \Delta^2$.

In the present study, we consider the case where the material properties of the ice are allowed to vary in space, i.e. $\alpha(x, y) = \alpha_0 + \alpha_c(x, y)$, $\beta(x, y) = \beta_0 +$

Description	Parameter	Values	Reference
Young's modulus	E	$7 \cdot 10^9 \text{ kg m}^{-1} \text{ s}^{-2}$	[80]
Poisson ratio	ν	0.33	[80]
Ice thickness	H	0.1 m – 1 km	[51, 42]
Density of seawater	ρ_{sea}	1025 kg m^{-3}	
Density of ice	ρ_{ice}	917 kg m^{-3}	
Gravitational acceleration	g	9.8 m s^{-2}	
Frequency	ω	$0.004 - 10 \text{ s}^{-1}$	[14, 8]

Table 1: Physical parameters of the model and their approximate values. The thickness of the ice can range from ordinary sea ice (0.1 - 4 m), to sea ice ridges (5 - 30 m), to Antarctic ice shelves (hundreds of meters to 1 km). The frequency of wave forcing can also vary dramatically – from low-frequency tsunami and infragravity waves (0.004 - 0.01 Hz), to ordinary gravity waves (0.05 - 1 Hz) and their higher resonances.

$\beta_c(x, y)$, and $\gamma(x, y) = \gamma$, where $\alpha_0 > 0$, $\beta_0 \in \mathbb{C}$, and $\gamma < 0$ are given constants, and α_c and β_c are compactly supported on a bounded region $\Omega \subset \mathbb{R}^2$. Note that the most common source of variation in these coefficients is changes in the thickness H ; however, the methods and analysis described here are sufficiently general to encompass contexts in which other material properties such as density or Young's modulus also vary. If $\Im(\beta_0) > 0$ then we say that the equations are in the dissipative regime, while if $\Im(\beta_0) = 0$ we say that they are in the non-dissipative regime.

The model given by (2.1) and (2.2) assumes infinite depth, which is appropriate when the fluid depth significantly exceeds the characteristic wavelength, as is the case for Arctic sea ice which sits above deep water where there is minimal interaction with the ocean floor [19]. This model also assumes the well-known shallow draft approximation [16], which allows one to treat the undersurface of the ice as the fixed surface $z = 0$ and assume that all thickness changes manifest in the upper surface of the ice (see Figure 1), even though such configurations may not be hydrostatically equilibrated. Previous studies that have looked at the effect of draft [65, 77] suggest that the governing equations depend merely on the distance between the keel and the sea bottom, so we do not expect the dynamics to be significantly altered in the infinite depth setting. Both the plate and fluid displacements are assumed to be small, allowing one to neglect quadratic terms in the equations of motion and fix the boundary.

3 Reduction to an integral equation

Suppose that a harmonic incident field ϕ^{inc} is prescribed and that $\phi = \phi^{\text{inc}} + \phi^{\text{scat}}$. The scattered field, ϕ^{scat} then satisfies

$$(\alpha \Delta_S^2 - \beta) \partial_z \phi^{\text{scat}} + \gamma \phi^{\text{scat}} = f, \quad z = 0, \quad (3.1)$$

where

$$f = -(\alpha\Delta_S^2 - \beta)\partial_z\phi^{\text{inc}} - \gamma\phi^{\text{inc}}.$$

We represent the scattered velocity potential ϕ^{scat} by a single layer potential with a charge density, σ , defined on the surface $z = 0$, i.e.

$$\phi^{\text{scat}}(\mathbf{r}_{3d}) = S[\sigma](\mathbf{r}_{3d}) := \text{p.v.} \int_{\mathbb{R}^2} \frac{1}{4\pi|\mathbf{r}_{3d} - \mathbf{r}'_{3d}|} \sigma(\mathbf{r}') dA(\mathbf{r}'), \quad (3.2)$$

where the principal value (p.v.) integral is defined as

$$\text{p.v.} \int_{\mathbb{R}^2} g(\mathbf{r}') dA(\mathbf{r}') = \lim_{R \rightarrow \infty} \int_{|\mathbf{r}'| \leq R} g(\mathbf{r}') dA(\mathbf{r}')$$

and

$$\mathbf{r}_{3d} = \begin{pmatrix} x \\ y \\ z \end{pmatrix}, \quad \mathbf{r}'_{3d} = \begin{pmatrix} x' \\ y' \\ 0 \end{pmatrix}, \quad \text{and} \quad \mathbf{r}' = \begin{pmatrix} x' \\ y' \end{pmatrix}.$$

Note that the p.v. integral is only necessary when the integrand is not absolutely integrable. The potential defined this way is harmonic and satisfies that $\partial_z\phi \rightarrow 0$ as $|\mathbf{r}_{3d}| \rightarrow \infty$ for any $\sigma \in L^2(\mathbb{R}^2)$. This reduces the problem to determining σ such that boundary condition (3.1) is satisfied.

Substituting the single layer representation of ϕ^{scat} into (3.1) and applying standard integral ‘‘jump formulas’’ in the limit $z \rightarrow 0^-$ yields

$$\frac{1}{2}(\alpha\Delta_S^2 - \beta)\sigma(\mathbf{r}) + \gamma \text{p.v.} \int_{\mathbb{R}^2} \frac{1}{4\pi|\mathbf{r} - \mathbf{r}'|} \sigma(\mathbf{r}') dA(\mathbf{r}') = f(\mathbf{r}), \quad (3.3)$$

for each $\mathbf{r} \in \mathbb{R}^2$. This is an integro-differential equation for σ . Note that a similar integro-differential equation in terms of plate displacement appears in [40] with some flexural terms omitted.

The remainder of this section derives an integral equation formulation for the surface problem (3.3). Section 3.1 describes an appropriate Green’s function for the constant coefficient case. Section 3.2 derives a variable coefficient integral equation for σ based on the (adjoint) Lippman-Schwinger formalism and the Green’s function of Section 3.1.

3.1 The constant coefficient problem

When the rigidity is constant, we have that $\Delta_S^2 = \Delta^2$. We consider the fundamental solution, G_S , of the constant coefficient version of (3.3), i.e.

$$(\alpha_0\Delta^2 - \beta_0)G_S(\mathbf{r}, \mathbf{r}') + \gamma \text{p.v.} \int_{\mathbb{R}^2} \frac{1}{2\pi|\mathbf{r} - \mathbf{r}''|} G_S(\mathbf{r}', \mathbf{r}'') dA(\mathbf{r}'') = 2\delta(\mathbf{r}, \mathbf{r}'), \quad (3.4)$$

where α_0 , β_0 , and γ are constants. We are also interested in the on-surface ($z = 0$) value of the single layer potential applied to this fundamental solution,

$$G_\phi(\mathbf{r}, \mathbf{r}') := \text{p.v.} \int_{\mathbb{R}^2} \frac{1}{4\pi|\mathbf{r} - \mathbf{r}''|} G_S(\mathbf{r}'', \mathbf{r}') dA(\mathbf{r}''), \quad (3.5)$$

which is the velocity potential corresponding to an impulse response.

The appropriate (outward radiating) solution of (3.4) can be derived via the limiting absorption principle. In particular, we first derive the solution of (3.4) for dissipative plates and take the limit from the complex upper half plane to obtain the appropriate radiating solution for real-valued β_0 .

Before stating the formulas, we require the following lemma that establishes some basic facts and notation related to the Fourier multiplier on the left hand side of (3.4). Its proof is straightforward and omitted.

Lemma 3.1. *Let ρ_1, \dots, ρ_5 denote the roots of the polynomial*

$$p(z) = \alpha_0 z^5 - \beta_0 z + \gamma. \quad (3.6)$$

If $\Im(\beta_0) \neq 0$, then none of the ρ_j are real. If $\beta_0 \in \mathbb{R}$, then exactly one of the ρ_j is a positive real number, which we label by ρ_1 .

Supposing that all of the roots are distinct, we define the coefficients e_1, \dots, e_5 by

$$e_j = \operatorname{Res}_{z=\rho_j} \frac{1}{p(z)} \quad \text{for each } j = 1, \dots, 5. \quad (3.7)$$

Additionally, the coefficients e_j and roots ρ_j satisfy the following relations

$$\sum_{j=1}^5 e_j \rho_j^q = 0 \text{ for } q \in \{0, 1, 2, 3, 5, 6, 7\}, \quad \sum_{j=1}^5 e_j \rho_j^4 = \frac{1}{\alpha_0}. \quad (3.8)$$

Remark 3.1. *The polynomial (3.6) corresponds to the deep water dispersion relation for flexural gravity waves [33, 58]. The moment relations (3.8) also appear in [73, 74]. The locations of the roots of (3.6) dictate the behavior of G_S at infinity. For ease of exposition, the formulas will be stated for the case that the roots ρ_1, \dots, ρ_5 are distinct. The results can easily be extended to the case in which two roots coincide (the form of the polynomial $p(z)$ precludes three or more roots coinciding). Details are given in appendix A.*

The following theorem provides an explicit formula for the fundamental solution of (3.4) and the corresponding velocity potential (3.5). Note that G_S also appears in a slightly different form in [32], and similar Green's functions appear in problems involving capillary surfers [25, 63].

Theorem 3.1. *Let the roots ρ_1, \dots, ρ_5 and the coefficients e_1, \dots, e_5 be as in the statement of Lemma 3.1 and suppose that the roots are distinct.*

If $\Im(\beta_0) \neq 0$, then

$$G_S(\mathbf{r}, \mathbf{r}') = \frac{1}{2} \sum_{j=1}^5 e_j \rho_j^2 \mathbf{K}_0(-\rho_j |\mathbf{r} - \mathbf{r}'|), \quad (3.9)$$

where \mathbf{K}_0 is the Struve function in standard notation [27]. For real-valued β_0 , consider the solution of (3.4) with β_0 replaced by $\beta_\epsilon = \beta_0 + i\epsilon$. The limit of G_S

as $\epsilon \rightarrow 0^+$ is

$$G_S(\mathbf{r}, \mathbf{r}') = \frac{1}{2} e_1 \rho_1^2 \left[-\mathbf{K}_0(\rho_1 |\mathbf{r} - \mathbf{r}'|) + 2i H_0^{(1)}(\rho_1 |\mathbf{r} - \mathbf{r}'|) \right] + \frac{1}{2} \sum_{j=2}^5 e_j \rho_j^2 \mathbf{K}_0(-\rho_j |\mathbf{r} - \mathbf{r}'|), \quad (3.10)$$

where $H_0^{(1)}$ is the Hankel function of the first kind.

The value of the corresponding velocity potential, given by (3.5), is

$$G_\phi(\mathbf{r}, \mathbf{r}') = \frac{1}{4} \sum_{j=1}^5 e_j \rho_j \mathbf{K}_0(-\rho_j |\mathbf{r} - \mathbf{r}'|) \quad (3.11)$$

in the case that $\Im(\beta_0) \neq 0$ and

$$G_\phi(\mathbf{r}, \mathbf{r}') = \frac{1}{4} e_1 \rho_1 \left[-\mathbf{K}_0(\rho_1 |\mathbf{r} - \mathbf{r}'|) + 2i H_0^{(1)}(\rho_1 |\mathbf{r} - \mathbf{r}'|) \right] + \frac{1}{4} \sum_{j=2}^5 e_j \rho_j \mathbf{K}_0(-\rho_j |\mathbf{r} - \mathbf{r}'|) \quad (3.12)$$

for real-valued β_0 .

Proof. The formula can be derived using Fourier analysis. See appendix A for details. \square

3.2 Variable coefficients

Recall that $\alpha(\mathbf{r}) = \alpha_0 + \alpha_c(\mathbf{r})$, $\beta(\mathbf{r}) = \beta_0 + \beta_c(\mathbf{r})$, where α_c and β_c are smooth functions which are compactly supported on $\Omega \subset \mathbb{R}^2$. We represent σ using

$$\sigma(\mathbf{r}) = \int_{\Omega} G_S(\mathbf{r}, \mathbf{r}') \mu(\mathbf{r}') dA(\mathbf{r}'), \quad (3.13)$$

where G_S is the Green's function from Theorem 3.1 for the constant parameters α_0 , β_0 , and γ . Substitution of this representation into (3.3) one obtains the adjoint Lippman-Schwinger equation:

$$\frac{\alpha}{\alpha_0} \mu(\mathbf{r}) + \frac{1}{2} \sum_{i=1}^8 \int_{\Omega} K_i(\mathbf{r}, \mathbf{r}') \mu(\mathbf{r}') dA(\mathbf{r}') = f(\mathbf{r}), \quad (3.14)$$

where the kernels K_i ($i = 1, \dots, 8$) in the integral equation above are defined by

$$K_1(\mathbf{r}, \mathbf{r}') = 2 \partial_x \alpha_c(\mathbf{r}) \partial_x \Delta_{\mathbf{r}} G_S(\mathbf{r}, \mathbf{r}') , \quad (3.15)$$

$$K_2(\mathbf{r}, \mathbf{r}') = 2 \partial_y \alpha_c(\mathbf{r}) \partial_y \Delta_{\mathbf{r}} G_S(\mathbf{r}, \mathbf{r}') , \quad (3.16)$$

$$K_3(\mathbf{r}, \mathbf{r}') = \Delta_{\mathbf{r}} \alpha_c(\mathbf{r}) \Delta_{\mathbf{r}} G_S(\mathbf{r}, \mathbf{r}') , \quad (3.17)$$

$$K_4(\mathbf{r}, \mathbf{r}') = -(1 - \nu) \partial_x^2 \alpha_c(\mathbf{r}) \partial_y^2 G_S(\mathbf{r}, \mathbf{r}') , \quad (3.18)$$

$$K_5(\mathbf{r}, \mathbf{r}') = -(1 - \nu) \partial_y^2 \alpha_c(\mathbf{r}) \partial_x^2 G_S(\mathbf{r}, \mathbf{r}') , \quad (3.19)$$

$$K_6(\mathbf{r}, \mathbf{r}') = 2(1 - \nu) \partial_{xy} \alpha_c(\mathbf{r}) \partial_{xy} G_S(\mathbf{r}, \mathbf{r}') , \quad (3.20)$$

$$K_7(\mathbf{r}, \mathbf{r}') = \frac{\alpha_c(\mathbf{r}) \beta_0 - \alpha_0 \beta_c(\mathbf{r})}{\alpha_0} G_S(\mathbf{r}, \mathbf{r}') , \quad (3.21)$$

$$K_8(\mathbf{r}, \mathbf{r}') = -\frac{\gamma \alpha_c(\mathbf{r})}{\alpha_0} G_\phi(\mathbf{r}, \mathbf{r}') , \quad (3.22)$$

and the righthand side is given by

$$f(\mathbf{r}) = -(\alpha \Delta_S^2 - \beta) \partial_z \phi^{\text{inc}} - \gamma \phi^{\text{inc}} . \quad (3.23)$$

If ϕ^{inc} satisfies the constant coefficient part of the PDE, then we are left with the righthand side:

$$\begin{aligned} f(\mathbf{r}) = & -(2 \nabla \alpha_c \cdot \nabla \Delta + (\Delta \alpha_c) \Delta + (1 - \nu)(2 \partial_{xy} \alpha_c \partial_{xy} - \partial_x^2 \alpha_c \partial_y^2 - \partial_y^2 \alpha_c \partial_x^2)) \partial_z \phi^{\text{inc}} \\ & - \left(\frac{\alpha_c}{\alpha_0} \beta_0 - \beta_c \right) \partial_z \phi^{\text{inc}} + \frac{\alpha_c}{\alpha_0} \gamma \phi^{\text{inc}} . \end{aligned}$$

Then we use the following representation(s) to obtain the total fields ϕ and $\partial_z \phi$ on the boundary $z = 0$:

$$\phi(\mathbf{r}) = \phi^{\text{inc}}(\mathbf{r}) + \int_{\mathbb{R}^2} G_\phi(\mathbf{r}, \mathbf{r}') \mu(\mathbf{r}') \, dA(\mathbf{r}') , \quad (3.24)$$

$$\partial_z \phi(\mathbf{r}) = \partial_z \phi^{\text{inc}}(\mathbf{r}) + \frac{1}{2} \int_{\mathbb{R}^2} G_S(\mathbf{r}, \mathbf{r}') \mu(\mathbf{r}') \, dA(\mathbf{r}') . \quad (3.25)$$

4 Analytical properties of the integral equation

In this section and the following one, we assume that the perturbations $\alpha_c, \beta_c \in C_c^\infty(\Omega)$. We also assume that the thickness H is always non-zero, so that $\alpha > 0$ everywhere in the domain.

4.1 Mapping properties of the integral equation

In this section we show that (3.14) is a second kind integral equation. The main analytical result is the following theorem.

Theorem 4.1. *Let $m \geq 0$. The integral operators associated with the kernels (3.15) to (3.22) map $H^m(\Omega) \rightarrow H^{m+1}(\Omega)$.*

Corollary 4.1. *The same operators are compact from $L^2(\Omega) \rightarrow L^2(\Omega)$.*

Corollary 4.2. Equation (3.14) is a Fredholm second kind integral equation on $L^2(\Omega)$.

Before proving Theorem 4.1, we require the following three lemmas. The first lemma, appearing in Section 6.3 of [31], pertains to the elliptic regularity of solutions to Poisson's equation and the second lemma is a straightforward extension to solutions of the inhomogeneous biharmonic equation. The third lemma, adapted from Proposition 4.4 of Chapter 4 of [75], pertains to the compact embedding of Sobolev spaces and establishes Corollary 4.1.

Lemma 4.1. Suppose that $f \in H^m(\Omega)$ and let $u \in H^1(\Omega)$ be a weak solution of the Poisson equation

$$\Delta u = f \quad x \in \Omega.$$

Then, $u \in H_{\text{loc}}^{m+2}(\Omega)$.

Lemma 4.2. Suppose that $f \in H^m(\Omega)$ and let $u \in H^3(\Omega)$ be a weak solution of the inhomogeneous biharmonic equation

$$\Delta^2 u = f \quad x \in \Omega.$$

Then, $u \in H_{\text{loc}}^{m+4}(\Omega)$.

Lemma 4.3 (Rellich). For any $s \geq 0, \sigma > 0$ the inclusion map

$$j : H^{s+\sigma}(\Omega) \rightarrow H^s(\Omega)$$

is compact.

We now proceed with the proof of Theorem 4.1.

Proof of Theorem 4.1. We present the details for the kernels (3.15) to (3.21) in the case that $\Im(\beta_0) = 0$. The arguments for $\Im(\beta_0) \neq 0$ and (3.22) are similar.

We first examine the asymptotics of (3.15) to (3.21) as $|\mathbf{r} - \mathbf{r}'| \rightarrow 0$. Recall the following power series expansions for the special functions $\mathbf{H}_0(\rho r)$, $Y_0(\rho r)$, and $J_0(\rho r)$ for $\rho \in \mathbb{C}$ (see [1]):

$$\mathbf{H}_0(\rho r) = \sum_{k=0}^{\infty} \frac{(-1)^k (\frac{1}{2}\rho r)^{2k+1}}{(\Gamma(k + \frac{3}{2}))^2}, \quad (4.1)$$

$$Y_0(\rho r) = \frac{2}{\pi} [\ln(\frac{1}{2}\rho r) + \gamma] J_0(\rho r) + \frac{2}{\pi} \sum_{k=1}^{\infty} (-1)^{k+1} H_k \frac{(\frac{1}{2}\rho r)^{2k}}{(k!)^2}, \quad (4.2)$$

$$J_0(\rho r) = \sum_{k=0}^{\infty} \frac{(-1)^k (\frac{1}{2}\rho r)^{2k}}{k! \Gamma(k+1)}, \quad (4.3)$$

where $\Gamma(x)$ is the gamma function, γ is the Euler-Mascheroni constant, and H_k is a harmonic number. Recall that $\mathbf{K}_n = \mathbf{H}_n - Y_n$ and $H_n^{(1)} = J_n + iY_n$.

From this we can show that the Green's function (3.10) has the power series expansion:

$$G_S(\mathbf{r}, \mathbf{r}') = \Psi_0(\mathbf{r}, \mathbf{r}') - \sum_{j=1}^5 e_j \rho_j^2 \left[\frac{1}{2\pi} \ln(|\mathbf{r} - \mathbf{r}'|^2) J_0(\rho_j |\mathbf{r} - \mathbf{r}'|) + \sum_{k=0}^{\infty} \frac{(-1)^k (\frac{1}{2} \rho_j |\mathbf{r} - \mathbf{r}'|)^{2k+1}}{2(\Gamma(k + \frac{3}{2}))^2} \right]$$

where $\Psi_0(\mathbf{r}, \mathbf{r}')$ is a smooth function given by:

$$\begin{aligned} \Psi_0(\mathbf{r}, \mathbf{r}') &= \frac{1}{\pi} e_1 \rho_1^2 [\ln(2/\rho_1) - \gamma + i\pi] J_0(\rho_1 |\mathbf{r} - \mathbf{r}'|) \\ &\quad + \sum_{j=2}^5 e_j \rho_j^2 \frac{1}{\pi} [\ln(-2/\rho_j) - \gamma] J_0(\rho_j |\mathbf{r} - \mathbf{r}'|) \\ &\quad + \frac{1}{\pi} \sum_{j=1}^5 \sum_{k=1}^{\infty} e_j \rho_j^2 (-1)^k H_k \frac{(\frac{1}{2} \rho_j |\mathbf{r} - \mathbf{r}'|)^{2k}}{(k!)^2}. \end{aligned}$$

Using the moment relations (3.8), one finds that the leading order behavior of G_S has the form:

$$\begin{aligned} G_S(\mathbf{r}, \mathbf{r}') &= \Psi_0(\mathbf{r}, \mathbf{r}') + \frac{1}{8\pi\alpha_0} |\mathbf{r} - \mathbf{r}'|^2 \ln(|\mathbf{r} - \mathbf{r}'|^2) + |\mathbf{r} - \mathbf{r}'|^7 \Psi_1(\mathbf{r}, \mathbf{r}') \\ &\quad + |\mathbf{r} - \mathbf{r}'|^6 \log(|\mathbf{r} - \mathbf{r}'|^2) \Psi_2(\mathbf{r}, \mathbf{r}'), \end{aligned}$$

where Ψ_1 and Ψ_2 are also smooth. Note that the leading order term is a scalar multiple of the Green's function for the biharmonic equation and the remaining terms have four continuous derivatives.

Now define the volume potential \mathcal{V} for the biharmonic equation in two dimensions as the integral operator

$$\mathcal{V}[\mu](\mathbf{r}) := \frac{1}{16\pi} \int_{\Omega} |\mathbf{r} - \mathbf{r}'|^2 \log(|\mathbf{r} - \mathbf{r}'|^2) \mu(\mathbf{r}') dA(\mathbf{r}'),$$

where $\mu \in H^m(\Omega)$. Let $u(\mathbf{r}) := \mathcal{V}[\mu](\mathbf{r})$. By Lemma 4.2, it must be that $u \in H_{\text{loc}}^{m+4}(\Omega)$. Likewise, for any kernel that is given as up to three derivatives of the biharmonic Green's function times some constant, we have that the corresponding integral operator maps $H^m(\Omega) \rightarrow H_{\text{loc}}^{m+1}(\Omega)$. By the decomposition of G_S above, integral operators defined for kernels with up to three derivatives of G_S have the same mapping properties.

The kernels (3.15) to (3.21) are each given as sums of kernels of the form $K(\mathbf{r}, \mathbf{r}') = \psi(\mathbf{r}) \tilde{K}(\mathbf{r}, \mathbf{r}')$ where $\psi(\mathbf{r})$ is a smooth, compactly supported function in Ω and \tilde{K} consists of up to third order derivatives of G_S . By the preceding, the integral operator for each kernel then maps $H^m(\Omega) \rightarrow H^{m+1}(\Omega)$. The argument of kernel (3.22) follows similarly. \square

4.2 Properties of the solutions of the integral equation

In this section, we show that solutions μ of the integral equation (3.14) have the same regularity as the data f , and that the surface density σ and its derivatives up to order four are as regular. We then show that σ satisfies certain decay and radiation conditions and that it is a solution of the original integro-differential equation (3.3).

Theorem 4.2. *Suppose that $m \geq 0$ and $f \in H_0^m(\Omega)$ and that $\mu \in L^2(\Omega)$ is a solution of (3.14). Then $\mu \in H_0^m(\Omega)$. Further, σ defined as in (3.13) has $\sigma \in H_{loc}^{m+4}(\mathbb{R}^2)$.*

Proof. Re-arranging (3.14), we have

$$\mu(\mathbf{r}) = \frac{\alpha_0}{\alpha} \left(f(\mathbf{r}) - \frac{1}{2} \sum_{i=1}^8 \int_{\mathbb{R}^2} K_i(\mathbf{r}, \mathbf{r}') \mu(\mathbf{r}') \, dA(\mathbf{r}') \right),$$

so that μ is the sum of $f \in H^m(\Omega)$ and a function that is smoother than μ . Applying induction, we have that $\mu \in H^m(\Omega)$. We observe also that the support of any output of the integral operators is contained in the support of α_c and β_c . Thus, $\mu \in H_0^m(\Omega)$.

Since $\mu \in H_0^m(\Omega)$ it can be extended to $\mu \in H^m(U)$ for any bounded domain U containing Ω . Arguing as in the proof of Theorem 4.1, the integral operator corresponding to the kernel G_S maps $H^m(U) \rightarrow H^{m+4}(U)$. Thus, $\sigma \in H_{loc}^{m+4}(\mathbb{R}^2)$. \square

Corollary 4.3. *Suppose that $f \in C_c^\infty(\Omega)$ and that $\mu \in L^2(\Omega)$ is a solution of (3.14). Then, $\mu \in C_c^\infty(\Omega)$ and σ defined as in (3.13) has $\sigma \in C^\infty(\mathbb{R}^2)$.*

In the case that the plate has some dissipation added, then σ decays sufficiently fast that quantities like the corresponding velocity potential can be defined using standard integrals. For the non-dissipative case, σ decays slowly but is an oscillatory, outgoing solution and the velocity potential defined by $S[\sigma]$ can be understood as a principal value integral.

Proposition 4.1. *Suppose that $\mu \in L^2(\Omega)$ and σ is defined as in (3.13). For $\Im(\beta_0) \neq 0$, we have*

$$\begin{aligned} \sigma &= \mathcal{O}(1/|\mathbf{r}|^3) \\ \text{and } \max(|\nabla\sigma|, |\nabla \otimes \nabla\sigma|, |\nabla \otimes \nabla \otimes \nabla\sigma|) &= \mathcal{O}(1/|\mathbf{r}|^4), \quad |\mathbf{r}| \rightarrow \infty. \end{aligned}$$

For $\Im(\beta_0) = 0$, we have

$$\frac{\mathbf{r}}{|\mathbf{r}|} \cdot \nabla\sigma - i\rho_1\sigma = o\left(1/\sqrt{|\mathbf{r}|}\right), \quad |\mathbf{r}| \rightarrow \infty, \quad (4.4)$$

where ρ_1 is the positive root of the dispersion relation, as in Lemma 3.1.

Proof. These decay properties follow from the asymptotic behavior of the kernel G_S and the fact that μ has bounded support. In particular, the Struve function \mathbf{K}_0 has the asymptotic expansion [1]

$$\mathbf{K}_0(z) \sim \frac{1}{\pi} \sum_{k=0}^{\infty} \frac{\Gamma(k + \frac{1}{2}) (\frac{1}{2}z)^{-2k-1}}{\Gamma(\frac{1}{2} - k)},$$

which is valid for large $|z|$. Applying the moment relations (3.7), we see that

$$G_S(\mathbf{r}, \mathbf{r}') = \mathcal{O}(1/|\mathbf{r}|^3)$$

for $\Im(\beta_0) \neq 0$ and

$$G_S(\mathbf{r}, \mathbf{r}') = ie_1 \rho_1^2 H_0^{(1)}(\rho_1 |\mathbf{r} - \mathbf{r}'|) + \mathcal{O}(1/|\mathbf{r}|^3)$$

for $\Im(\beta_0) = 0$. The decay for the derivatives can be derived similarly. \square

Corollary 4.4. *Suppose that $f \in L^2(\Omega)$ and $\mu \in L^2(\Omega)$ is a solution of (3.14). Then, σ defined as in (3.13) is a solution of (3.3) and $S[\sigma]$ is a solution of the boundary value problem (2.1) and (2.2).*

5 Existence and uniqueness of solutions of the integral equations

In this section, Ω is a bounded domain with smooth boundary containing the support of f . As before, let α be a smooth, positive function that is compactly supported on Ω . For the results in this section, we also require the following property:

Property 5.1 (Dissipative regime). *Suppose $\beta(x, y) = \beta_0 + \beta_c(x, y)$, where $\beta_0 \in \mathbb{C}$ and $\beta_c(x, y) \in C_c^\infty(\Omega)$. We say that the parameters are in the dissipative regime if $\Im(\beta_0) > 0$.*

The main results of this section establish the existence and uniqueness of solutions of the boundary value problem (2.1) and (2.2) in this regime. For real-valued β_0 we show that a unique solution of the integral equation (3.14) exists except, possibly, for a set of nowhere dense values of β_0 .

Theorem 5.1. *Suppose Ω is a bounded domain with smooth boundary and that β satisfies Property 5.1. Let $f \in L^2(\Omega)$ be given. Then, the integral equation (3.14) for μ has a unique solution. For real-valued β_0 , (3.14) has unique solutions except, possibly, for a set of nowhere dense values.*

Corollary 5.1. *Suppose Ω is a bounded domain with smooth boundary and that β satisfies Property 5.1. Let $f \in L^2(\Omega)$ be given. Then, the boundary value problem (2.1) and (2.2) has a unique solution satisfying the decay conditions in Proposition 5.1. For real-valued β_0 , the boundary value problem has a solution except, possibly, for a set of nowhere dense values.*

Before proving Theorem 5.1, we require some preliminary results. The first preliminary result establishes the uniqueness of solutions of the boundary value problem in the dissipative regime, assuming appropriate decay conditions.

Proposition 5.1. *Assume that the coefficient β satisfies Property 5.1. Let $\phi \in H_{loc}^2(z < 0)$ be a solution of the homogeneous ($f = 0$) version of (2.1) and (2.2), which has its normal trace in $H_{loc}^4(\mathbb{R}^2)$ and satisfies the following decay conditions*

$$\begin{aligned} |\phi(\mathbf{r}_{3d})| &= \mathcal{O}(1/|\mathbf{r}_{3d}|) & |\mathbf{r}_{3d}| \rightarrow \infty \\ \left| \frac{\mathbf{r}_{3d}}{|\mathbf{r}_{3d}|} \cdot \nabla_{3d} \phi(\mathbf{r}_{3d}) \right| &= \mathcal{O}(1/|\mathbf{r}_{3d}|^2) & |\mathbf{r}_{3d}| \rightarrow \infty \\ \max(|\nabla \partial_z \phi|, |\nabla \otimes \nabla \partial_z \phi|, |\nabla \otimes \nabla \otimes \nabla \partial_z \phi|) &= \mathcal{O}(1/|\mathbf{r}|^2) & z = 0, \quad |\mathbf{r}| \rightarrow \infty. \end{aligned}$$

Then $\phi \equiv 0$.

Proof. Suppose that ϕ satisfies the conditions of the theorem. For given $R > 0$, let $\Omega_R = \{\mathbf{r}_{3d} = (x, y, z) : |\mathbf{r}_{3d}| < R \text{ and } z < 0\}$.

Let $\partial\Omega_R = D_R \cup H_R$ where D_R is the disc of radius R in the plane $z = 0$ and H_R is the lower hemisphere of radius R .

Then

$$\begin{aligned} 0 &= \int_{\Omega_R} \phi \Delta_{3d} \bar{\phi} - \bar{\phi} \Delta_{3d} \phi \, dV \\ &= \int_{H_R} \phi \bar{\phi}_n - \bar{\phi} \phi_n \, dS + \int_{D_R} \phi \bar{\phi}_z - \bar{\phi} \phi_z \, dA. \end{aligned}$$

The decay conditions imply that the first integral tends to zero as $R \rightarrow \infty$.

For $z = 0$, we have $\phi = -\alpha/\gamma \Delta_S^2 \phi_z + \beta/\gamma \phi_z$. Thus, the integral over D_R becomes

$$\begin{aligned} \int_{D_R} \phi \bar{\phi}_z - \bar{\phi} \phi_z \, dA &= -\frac{1}{\gamma} \int_{D_R} (\alpha \Delta_S^2 - \beta) \phi_z \bar{\phi}_z - (\alpha \Delta_S^2 - \bar{\beta}) \bar{\phi}_z \phi_z \, dA \\ &= \frac{2i\Im(\beta_0)}{\gamma} \int_{D_R} |\phi_z|^2 \, dA - \frac{1}{\gamma} \int_{D_R} \bar{\phi}_z \alpha \Delta_S^2 \phi_z - \phi_z \alpha \Delta_S^2 \bar{\phi}_z \, dA \end{aligned}$$

Integration by parts together with the in-plane decay conditions imply that the second term tends to zero as $R \rightarrow \infty$ (see, e.g. [50], Chapter 11 §12).

We then obtain that

$$0 = \frac{2i\Im(\beta_0)}{\gamma} \int_{D_R} |\phi_z|^2 \, dA$$

so that $\phi_z \equiv 0$ on the surface $z = 0$. But then the boundary condition on $z = 0$ implies that $\phi = 0$ there as well. We see that ϕ is a bounded solution of the half-space Dirichlet problem and is thus 0 everywhere. \square

The second preliminary result concerns the decay of single layer potentials for densities defined on the plane $z = 0$ that satisfy certain decay conditions.

Lemma 5.1. *Suppose that $\sigma \in L^2(\mathbb{R}^2)$ is continuously differentiable and that*

$$\sigma(\mathbf{r}) = \mathcal{O}(1/|\mathbf{r}|^3) \quad \text{and} \quad |\nabla\sigma(\mathbf{r})| = \mathcal{O}(1/|\mathbf{r}|^4).$$

Then,

$$S[\sigma](\mathbf{r}_{3d}) = \mathcal{O}(1/|\mathbf{r}_{3d}|) \quad \text{and} \quad \left| \frac{\mathbf{r}_{3d}}{|\mathbf{r}_{3d}|} \cdot \nabla_{3d} S[\sigma](\mathbf{r}_{3d}) \right| = \mathcal{O}(1/|\mathbf{r}_{3d}|^2) \quad \text{as } |\mathbf{r}_{3d}| \rightarrow \infty.$$

Proof. Let σ satisfy the assumptions above. For $R > 0$, let D_R denote the disc of radius R in \mathbb{R}^2 . Let $G(\mathbf{r}_{3d}, \mathbf{r}'_{3d}) = 1/(4\pi|\mathbf{r}_{3d} - \mathbf{r}'_{3d}|)$. Let $\mathbf{r}_{3d} \neq 0$ in \mathbb{R}^3 and let $R = |\mathbf{r}_{3d}|/2$.

We divide the integrals over \mathbb{R}^2 in the definition of $S[\sigma]$ and $\nabla_{3d} S[\sigma]$ into three parts: the disc D_R , the annulus $A_{R,4R} = D_{4R} \setminus D_R$, and the disc exterior $E_{4R} = \mathbb{R}^2 \setminus D_{4R}$. Let $n(\mathbf{r})$ denote the outward normal at $\mathbf{r} \in \partial A_{R,4R}$.

The decay conditions on σ imply that $\sigma \in L^1(\mathbb{R}^2)$. For the contribution over D_R , standard multipole estimates then imply that

$$\left| \int_{D_R} G(\mathbf{r}_{3d}, \mathbf{r}'_{3d}) \sigma(\mathbf{r}') \, dA(\mathbf{r}') \right| = \mathcal{O}(1/R) \quad \text{and} \\ \left| \int_{D_R} \nabla_{3d} G(\mathbf{r}_{3d}, \mathbf{r}'_{3d}) \sigma(\mathbf{r}') \, dA \right| = \mathcal{O}(1/R^2).$$

If $\mathbf{r}' \in E_{4R}$, then $G(\mathbf{r}_{3d}, \mathbf{r}'_{3d}) = \mathcal{O}(1/R)$ and $\nabla_{3d} G(\mathbf{r}_{3d}, \mathbf{r}'_{3d}) = \mathcal{O}(1/R^2)$. Because σ is integrable over \mathbb{R}^2 , the contribution over E_{4R} then has the same bound.

We note that $\sigma(\mathbf{r}') = \mathcal{O}(1/R^3)$ for $\mathbf{r}' \in A_{R,4R}$. We also have that

$$\int_{A_{R,4R}} G(\mathbf{r}_{3d}, \mathbf{r}'_{3d}) \, dA(\mathbf{r}') \leq \int_{A_{R,4R}} \frac{1}{4\pi|\mathbf{r} - \mathbf{r}'|} \, dA(\mathbf{r}') \\ \leq \int_{D_1} \frac{1}{4\pi|\mathbf{r}'|} \, dA(\mathbf{r}') + \frac{1}{4\pi} \int_{A_{R,4R}} \, dA(\mathbf{r}') \leq \frac{1}{2} + \frac{15}{4} R^2.$$

where \mathbf{r} is the projection of \mathbf{r}_{3d} onto $z = 0$. Thus, the contribution over $A_{R,4R}$ is $\mathcal{O}(1/R)$ for $S[\sigma]$. For the directional derivative, we split the estimate into two pieces. We have

$$\frac{\mathbf{r}_{3d}}{|\mathbf{r}_{3d}|} \cdot \left(-\frac{\mathbf{r}_{3d} - \mathbf{r}'_{3d}}{4\pi|\mathbf{r}_{3d} - \mathbf{r}'_{3d}|^3} \right) \\ = -\frac{z^2}{4\pi|\mathbf{r}_{3d}||\mathbf{r}_{3d} - \mathbf{r}'_{3d}|^3} + \frac{\mathbf{r}}{|\mathbf{r}_{3d}|} \cdot \nabla \frac{1}{4\pi\sqrt{z^2 + (x-x')^2 + (y-y')^2}},$$

where $\nabla = (\frac{\partial}{\partial x}, \frac{\partial}{\partial y})$. For the first piece, we have

$$\left| -\frac{z^2}{4\pi|\mathbf{r}_{3d}||\mathbf{r}_{3d} - \mathbf{r}'_{3d}|^3} \right| \leq \frac{1}{8\pi R} \frac{1}{|\mathbf{r}_{3d} - \mathbf{r}'_{3d}|}.$$

We can then use the same estimate for the integral of $G(\mathbf{r}_{3d}, \mathbf{r}'_{3d})$ over the annulus to obtain that the contribution for this part is $\mathcal{O}(1/R^2)$.

For the second piece, we have that

$$\begin{aligned} & \int_{A_{R,4R}} \nabla \frac{1}{4\pi\sqrt{z^2 + (x-x')^2 + (y-y')^2}} \sigma(\mathbf{r}') \, dA(\mathbf{r}') \\ &= - \int_{A_{R,4R}} \frac{1}{4\pi\sqrt{z^2 + (x-x')^2 + (y-y')^2}} \nabla \sigma(\mathbf{r}') \, dA(\mathbf{r}') \\ &+ \int_{\partial A_{R,4R}} \frac{1}{4\pi\sqrt{z^2 + (x-x')^2 + (y-y')^2}} \sigma(\mathbf{r}') n(\mathbf{r}') \, d\ell(\mathbf{r}') \\ &= \mathcal{O}(1/R^2). \end{aligned}$$

□

The final preliminary result establishes the injectivity of convolution with G_S in the dissipative regime.

Lemma 5.2. *Suppose that α, β, γ satisfy Property 5.1. The operator $\mu \rightarrow G_S * \mu$ is injective from $L^2(\Omega)$ to $L^2(\mathbb{R}^2)$ for any bounded domain $\Omega \subset \mathbb{R}^2$.*

Proof. Any function $\mu \in L^2(\Omega)$ has a well-defined Fourier transform, $\hat{\mu}$, in $L^2(\mathbb{R}^2)$. The given operator has a Fourier multiplier which is bounded and continuous and its only zero is at the origin. Thus, the Fourier transform of $G_S * \mu$ is zero only if $\hat{\mu}$ is zero and so the convolution is zero only if μ is zero. □

We now proceed with the proof of Theorem 5.1.

Proof of Theorem 5.1. We first consider the case in which Property 5.1 holds. Under these assumptions, the integral equation is Fredholm on $L^2(\Omega)$. Thus, the existence of solutions can be reduced to uniqueness of solutions. Suppose that $\mu \in L^2(\Omega)$ is a solution of the homogeneous equation. Then $\sigma = G_S * \mu$ solves the homogeneous integro-differential equation and satisfies the decay conditions described in Proposition 4.1. Applying Corollary 4.4 and Lemma 5.1, we obtain that $S[\sigma]$ is a solution of the original PDE that satisfies the conditions of Proposition 5.1. Thus, $S[\sigma] \equiv 0$ in the lower half space. But in fact, $S[\sigma]$ is bounded throughout space by Lemma 5.1 and by continuity satisfies the homogeneous Dirichlet boundary condition in the upper half space as well. Thus, $S[\sigma] \equiv 0$ in \mathbb{R}^3 . By considering the difference of the limiting normal derivatives from the upper and lower half-spaces, we obtain that $\sigma \equiv 0$. But then $G_S * \mu \equiv 0$ and $\mu \equiv 0$ by Lemma 5.2. Applying the Fredholm alternative, we see that the integral equation has a unique solution for any $f \in L^2(\Omega)$.

Finally, we turn to the case of $\beta_0 \in \mathbb{R}$. We begin by noting that the kernels K_i in (3.14), as functions of β_0 , can be analytically continued from $\Im(\beta_0) > 0$ to an open neighborhood of $\mathbb{R} \subset \mathbb{C}$; see Proposition A.1 for details. Moreover, the operators remain compact from $L^2(\Omega) \rightarrow L^2(\Omega)$. Thus, the operator on the left-hand side of (3.14) is Fredholm, analytic, and invertible at a point in an

open neighborhood of \mathbb{R} and hence, by the Generalized Steinberg's theorem, has a bounded inverse for all β_0 in a neighborhood of \mathbb{R} except possibly for certain isolated points [34, 2]. \square

6 Numerical implementation and fast algorithms

In this section, we describe the numerical discretization and solution of the integral equation (3.14), establish the convergence properties of the method, and report tests that were performed to confirm the accuracy and convergence of the implementation.

6.1 Discretization, quadrature rule, and fast solution

We use a Nyström method to discretize (3.14). In particular, the grid points are taken to be equispaced points of the form $\mathbf{x}_i^h = (hi_1, hi_2)$ where $|i_1| < N_x$ and $|i_2| < N_y$ for some N_x and N_y sufficiently large that $\Omega \subset [hN_x, hN_y]$, i.e. that the grid covers the support of α_c and β_c . For such a grid, it is well-known that the trapezoidal rule, i.e.

$$\int_{\Omega} g(\mathbf{r}) dA(\mathbf{r}) \approx \sum_{|i_1| < N_x, |i_2| < N_y} g(\mathbf{x}_i^h) h^2,$$

has an error that decays super-algebraically for $g \in C_c^\infty(\Omega)$.

Each kernel in (3.14) can be written as $K_j(\mathbf{r}, \mathbf{r}') = \beta_j(\mathbf{r})w_j(\mathbf{r} - \mathbf{r}')$, where $\beta_j \in C_c^\infty(\Omega)$ and w_j is G_ϕ , G_S , or a derivative of G_S . These kernels are weakly singular, so we must modify the trapezoidal rule to obtain high-order accuracy. In particular, we seek a locally modified trapezoidal rule that consists of a set of indices, \mathcal{C} , centered around $(0, 0)$ and a set of modified weights, $\alpha_i^j(h)$, for each K_j such that the quadrature rule

$$\begin{aligned} & \int_{\Omega} K_j(\mathbf{x}_i^h, \mathbf{r}') \mu(\mathbf{r}') dA(\mathbf{r}') \\ & \approx \beta_j(\mathbf{x}_i^h) \left(\sum_{\mathbf{i}-\mathbf{i}' \in \mathcal{C}} \alpha_{\mathbf{i}-\mathbf{i}'}^j(h) \mu(\mathbf{x}_{\mathbf{i}'}^h) + h^2 \sum_{\mathbf{i}-\mathbf{i}' \notin \mathcal{C}} w_j(\mathbf{x}_i^h - \mathbf{x}_{\mathbf{i}'}^h) \mu(\mathbf{x}_{\mathbf{i}'}^h) \right) \end{aligned} \quad (6.1)$$

has an error that is $\mathcal{O}(h^p)$ for some reasonably large p . The weights should also satisfy a stability property, i.e.

$$\max_{j=1, \dots, 8} \sum_{\mathbf{i} \in \mathcal{C}} |\alpha_{\mathbf{i}}^j(h)| = \mathcal{O}(h). \quad (6.2)$$

Such quadrature rules can be obtained using the Zeta-corrected theory developed in [82, 83, 84, 43]. These methods compute integrals of the form

$$I = \int_{\Omega} \frac{g(\mathbf{r})}{|\mathbf{r} - \mathbf{x}_i^h|^s} dA(\mathbf{r}), \quad I = \int_{\Omega} g(\mathbf{r}) \log |\mathbf{r} - \mathbf{x}_i^h| dA(\mathbf{r}),$$

for $s \in \mathbb{R}$ and $g \in C_c^\infty(\Omega)$. In particular, when g is a monomial, it is possible to show that the error in approximating the integrals above is given exactly by the Epstein-Zeta function (or derivatives thereof). A moment-fitting method can then be used to obtain modifications of the trapezoidal rule that only affect a small number of grid points near \mathbf{x}_i^h , i.e. $|\mathcal{C}|$ is relatively small, and compute the integrals to a given order of accuracy. While previous work has focused primarily on Laplace, Helmholtz, and Stokes kernels [83, 84], a straightforward extension of this procedure can be used to obtain high-order quadratures for the biharmonic ($|\mathbf{r}|^2 \log |\mathbf{r}|$) kernel and its derivatives up to order three (see code for more details). For the calculations in this paper, we use order $p = 6$ for these corrections.

Remark 6.1. *As noted above, the Green's function G_S can be expressed as a constant, plus a smooth multiple of the biharmonic kernel and a smooth multiple of $|\mathbf{r}|^7$. Owing to the symmetries of the quadrature rules, the stability property of the modified weights, and a further modification at $(0,0)$ to handle the constant term, a sufficiently high-order Zeta-corrected rule for the biharmonic kernel or any of its derivatives up to order three will result in a 6th-order accurate rule for G_S or its corresponding derivative. Hence, we employ a 6th-order rule derived for the biharmonic kernel to discretize our integral operators.*

As confirmation of the numerical implementation of the quadrature rules, the quadrature corrections were verified numerically by applying the integral operators to a test density μ for various grid spacings h . The test density was chosen to be a scaled Gaussian so that the density decays to machine epsilon within the domain of discretization. The integral was measured at a fixed target at another point on the grid. In lieu of an analytic expression for the true value, we compare with reference values obtained using Matlab's adaptive integration routine. The results are shown in fig. 2.

Remark 6.2. *While the kernels found in the integral equation (3.14) are at most weakly singular, a naive implementation of the evaluation of these kernels will lead to catastrophic cancellation. This is due to the fact that the Hankel and Struve terms in the Green's function (3.10) possess log singularities which are canceled out by the moment relations (3.8). In the proof of Theorem 4.1, it was shown that these log singularities cancel out and the leading order behavior of $G_S \sim r^2 \log r$. The effect of these cancellations is further exacerbated by the derivatives which are applied to the Green's function in the kernel, which would lead the log terms of the Hankel and Struve functions to become $O(\frac{1}{|\mathbf{r}|^3})$. To remedy this, stable evaluators were made for $\frac{i}{4}H_0^{(1)}(x) + \frac{1}{2\pi} \log(x)$ and $\mathbf{K}_0(x) - \frac{2}{\pi} \log(x)$ and all of their derivatives up to order 3. This is done by evaluating the asymptotic expansions near zero (4.1)-(4.3) whenever the argument is small with the log term canceled explicitly.*

Because the kernels, w_j , appearing in the integral operators are translationally invariant, the quadrature rule, (6.1), for K_j is in the form of a discrete convolution (Toeplitz matrix product) followed by diagonal multiplication by

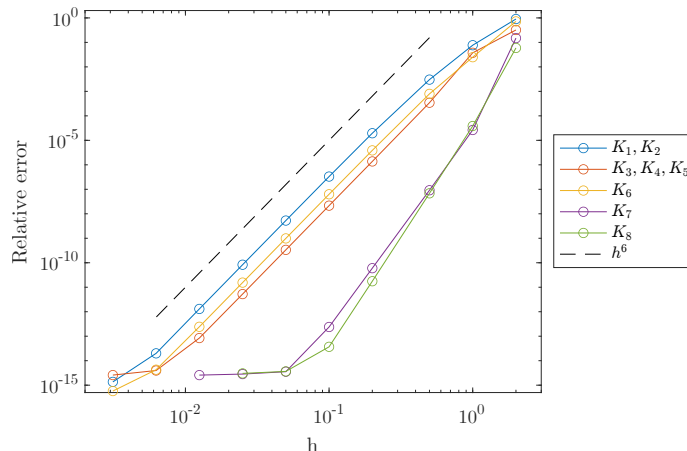


Figure 2: Convergence of discretized integral operators from equation (3.14) computed using trapezoid rule with 6th-order Zeta corrections.

the $\beta_j(\mathbf{x}_i^h)$ values. It is well-known that the FFT can then be used to reduce the complexity of performing this product from $\mathcal{O}(N_x^2 N_y^2)$ to $\mathcal{O}(N_x N_y (\log N_x + \log N_y))$. This speed-up in the application of the discretized integral operators makes the system well-suited to solution by an iterative solver such as GMRES. This technique has previously been used in a number of other contexts, particularly in the solution of the Lippman-Schwinger equation for the Helmholtz scattering problem; see, *inter alia*, [28, 36] and the references therein.

6.2 Convergence of the numerical method

It can be shown that the solution of the discrete linear system corresponding to the integral equation will converge to the solution of the continuous integral equation with the same convergence rate as the quadrature rule. Specifically, we have the following proposition.

Proposition 6.1. *Let $f \in C_c^\infty(\Omega)$ and let μ be the solution to (3.14). Furthermore, suppose μ^h is the solution to the discretized equation using a p -th order modified trapezoidal rule on a grid with spacing h , as in (6.1), to discretize the integral operators and suppose that the quadrature rule satisfies the stability condition (6.2). Let $\{\mathbf{x}_i^h\}$ denote the corresponding discretization nodes. If the operator on the left-hand side of (3.14) has a bounded inverse, then there exists an $h_0 > 0$ such that the discrete system is invertible for all $0 < h < h_0$. Moreover, there exists a constant C such that*

$$\max_i |\mu(\mathbf{x}_i^h) - \mu_i^h| \leq Ch^p$$

for all $0 < h < h_0$.

Proof. Invertibility of the discrete system follows directly from Theorem D.1, and Corollary D.1, while the rate of convergence follows from Theorem D.2, proved in the appendix. \square

To check the accuracy of the solutions to the integral equation we apply two different tests. In both tests, we send a plane wave with wavenumber $k = 1.05$ toward a Gaussian thickness profile with width $\sigma = 4$ m and height $A = 2$ m. In the first test, we solve (3.14) for the density μ and then use the FFT to interpolate the density onto a fine grid ($h_{\text{fine}} = 0.0625$). The interpolated density is then used to compute the solution ϕ on the same grid. After computing the solutions for different h on the fine grid, we can use high-order finite differences to check the consistency of the solution with the original PDE boundary condition (2.2). In particular, the residual of the boundary condition was computed at the surface points $\{(m/2, n/2) \mid -8 \leq m, n \leq 8\}$ and divided by the largest term in the boundary condition in order to get the relative errors. The ℓ^2 and ℓ^∞ norms of these relative errors are displayed in fig. 3. For the second test, we compute the backward error in the integral equation by comparing the density interpolated on an even finer grid ($h_{\text{finest}} = 0.015625$) with the converged density using both L^2 and L^∞ norms. Because this test does not rely on finite differences, it continues to converge even after the finite difference test has stalled.

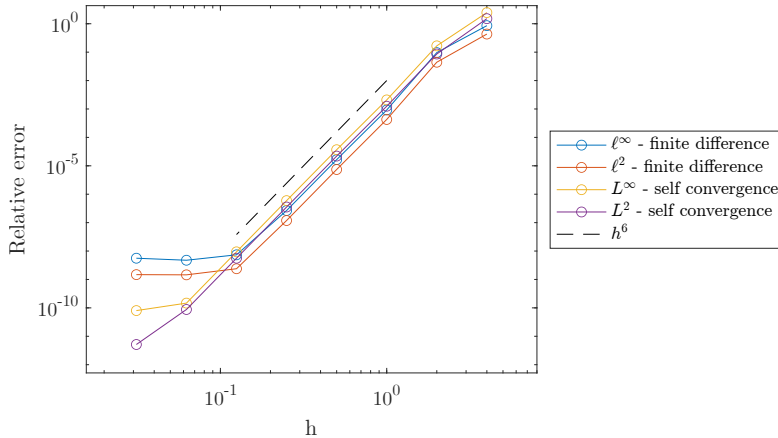


Figure 3: Convergence of the solution to the integral equation (3.14) for a Gaussian thickness profile and incident plane wave. The consistency of the solution ϕ with the surface PDE (2.2) is shown in red and blue, while the self-convergence of the density μ is shown in yellow and purple.

7 Examples and applications

In this section, we present some numerical examples of flexural-gravity wave scattering problems that are inspired by glaciology. For each of the examples, the consistency with the PDE was checked using finite differences, and the relative error in each case was measured to be around $1e-6$.

In the first example, we look at what happens to a point source inside of a random medium, which is inspired by the highly heterogeneous nature of sea ice and ice shelves (fig. 4). To generate the random medium, a collection of Gaussians were placed at a regular interval and added to a mean thickness profile of 5 m. The amplitude of each Gaussian was sampled from a uniform distribution on the interval $[-1, 1]$, the standard deviation of each Gaussian was chosen to be 75 m, and each Gaussian was placed one standard deviation apart on a 12 km by 12 km domain. Then, the right-hand side was chosen to be a point source with frequency 1 Hz ($k = 0.0255 \text{ m}^{-1}$) using the Green's function centered in the middle of the domain. As the wave energy propagates through the random medium, the wave begins to branch out in different directions; this wave branching phenomenon has previously been reported in [44, 45, 62]. The resulting interference pattern is produced by diffuse reflection through a highly heterogeneous medium.

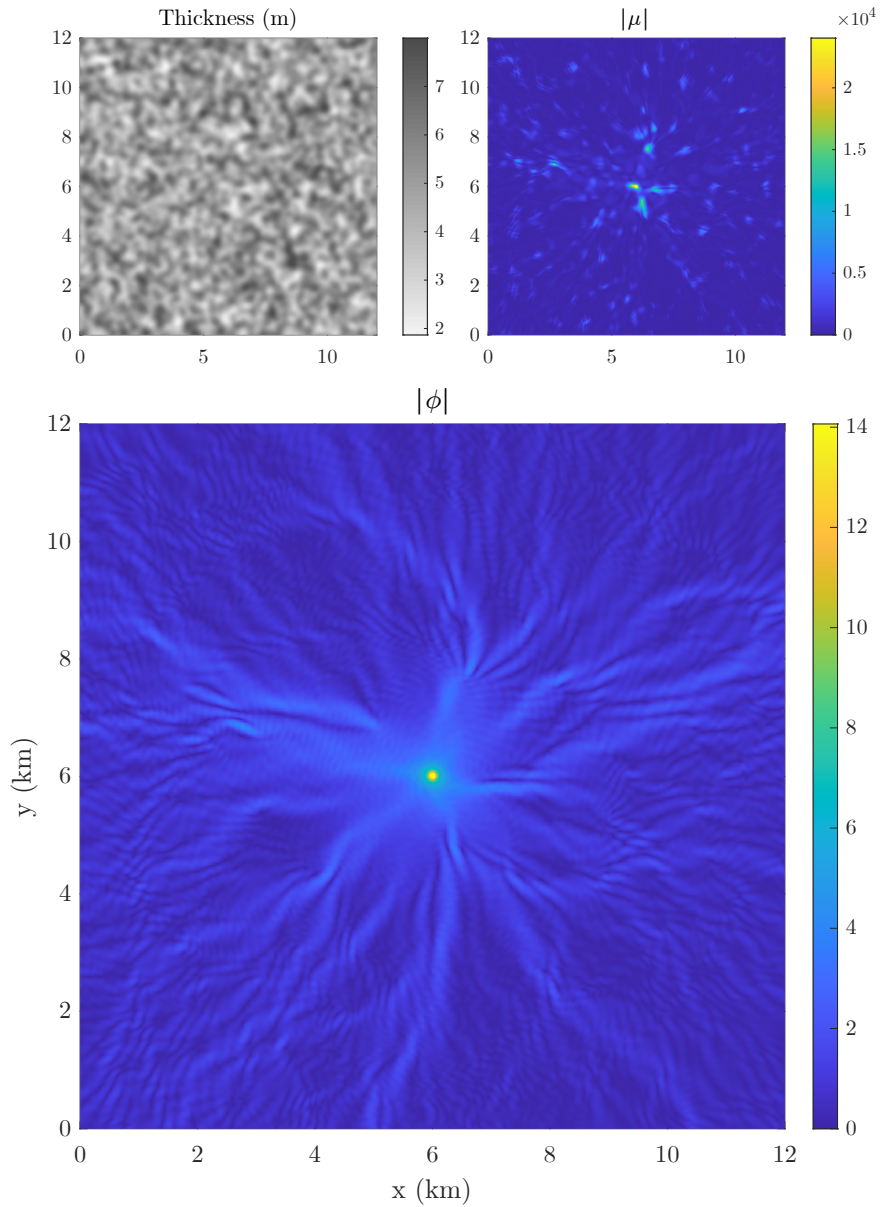


Figure 4: A point source inside of a random flexural medium. Top left: thickness profile generated by a sum of Gaussian distributions with random height values. The average thickness is 5 m. Top right: the absolute value of the density μ . This density can be viewed as the strength of sources that must be added to the original point source to produce the total field. Bottom: the absolute value of the velocity potential for a point source radiating outwards from the center of the domain.

Next, we examine the effect of sinusoidal variations in thickness on the propagation of flexural waves fig. 5. Such undulations can be found in the surface rolls of Arctic ice shelves [61] and the rumples of Antarctic ice shelves [23]. These rolls are believed to be formed by compressive wrinkling of a thin ice layer, though the exact mechanism is largely unknown. For this study, the thickness $H(x, y)$ is based on the amplitude of the surface roll pattern A and the observed freeboard H_f :

$$H(x, y) = \frac{\rho_{\text{sea}}}{\rho_{\text{sea}} - \rho_{\text{ice}}} \left[\left(\frac{A}{2} + \frac{A}{2} \sin(2\pi x/w) \right) \psi(x, y) + H_f \right],$$

where w is the width of each roll and $\psi(x, y)$ is a smooth tapering function given by

$$\psi(x, y) = (\text{erf}(s(x - x_0)) + \text{erf}(s(x_1 - x)))(\text{erf}(s(y - y_0)) + \text{erf}(s(y_1 - y)))$$

This function is almost unity on the region $[x_0, x_1] \times [y_0, y_1]$ and smoothly decays outside this region, ensuring that the pattern is compactly supported. The parameter s controls the rate at which the pattern transitions between one and zero. For this study, we consider realistic values $A = 0.75$ m, $w = 333.3$ m, $H_f = 0.35$ m, $s = 0.008$. We send in horizontal plane waves that sweep a range of wavenumbers between $0.001 - 0.06$ m⁻¹ and measure the amplitude of the solution at two different points before and after the roll pattern as a proxy for the reflected and transmitted field (fig. 5).

This frequency sweep demonstrates the degree to which the qualitative wave behavior is sensitive to the incident wavenumber. For both low and high wavenumbers, the incident wave is mostly transmitted with very little reflection. At times, the amplitude of the transmitted field exceeds one due to lateral scattering effects at the top and bottom boundaries of the roll geometry. At intermediate wavenumbers, the reflection and transmission vary dramatically, with the reflected component shooting up at intermittent values of k . This type of variation in the reflection is sometimes referred to as a resonance comb [73]. There are a few wavenumbers where the field is almost entirely reflected, owing to a phenomenon known as Bragg scattering. One of these fields is plotted in fig. 6, contrasted against a similar wavenumber for which the field is mostly transmitted.

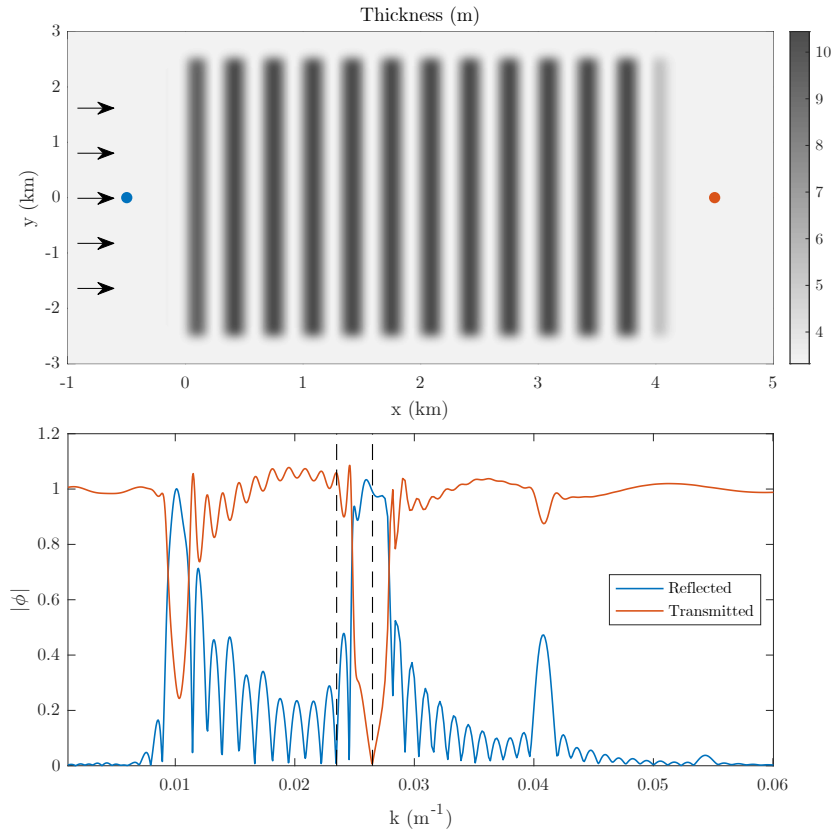


Figure 5: Top: surface roll pattern with a wavelength of 333 m. Arrows indicate direction of the incident plane wave. The blue dot indicates where the scattered field was measured as a proxy for the amplitude of the reflected wave, while the red dot marks the location where the total field was measured for the amplitude of the transmitted wave. Bottom: amplitudes of the reflected and transmitted fields for a wide range of wavenumbers. Dashed lines represent wavenumbers values that are plotted in fig. 6.

We now turn to an example of scattering by a system of pressure ridges (fig. 7). In contrast with the previous example, these ridges are not parallel but are allowed to branch outward in different directions. Such ridge systems are commonly found in the Arctic, and there are many mysteries associated with the formation and orientation of these ridges. In this example, we create these ridges by convolving the Gaussian kernel with a constant density defined on some piecewise curves. Getting the derivatives of this thickness profile simply amounts to taking derivatives of the Gaussian kernel. We allow these ridges to have a thickness of 3 m while the background thickness is 1 m. Then, we send an incident plane wave with a wavenumber of $k = 0.13 \text{ m}^{-1}$. The wave is scattered upon contact with each successive branch of the ridge pattern, suggesting that

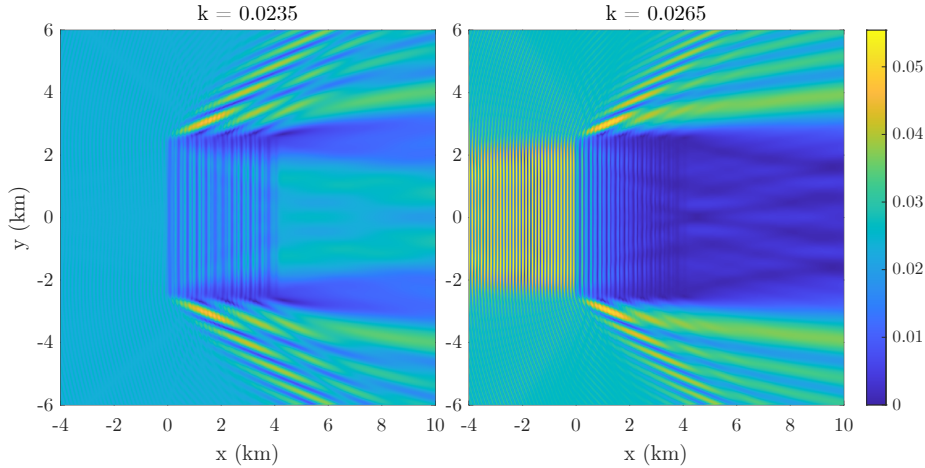


Figure 6: Wave scattering by an array of sinusoidal rolls for two similar wavenumbers. The quantity that is plotted is the absolute value of the velocity $|\phi_z|$. Left: a solution with wavenumber $k = 0.0235$ where most of the wave energy is transmitted. Right: a solution with wavenumber $k = 0.0265$ where most of the wave energy is reflected.

wave-ice interaction is significantly complicated by the presence of ridges.

In the next example we look at wave interaction with a spiral-shaped channel or groove in the ice (fig. 8). This groove is parametrized using the following formula:

$$\mathbf{r}_s(t) = (-at^3 \cos(t), at^3 \sin(t))$$

where $a = 0.0001$. Then, the thickness H is given by the following convolution of the speed of the curve with the Gaussian kernel:

$$H(\mathbf{r}) = H_0 + A \int_{5\pi}^{11\pi} \exp\left(\frac{-|\mathbf{r} - \mathbf{r}_s(t)|^2}{2\sigma^2}\right) |\mathbf{r}'_s(t)| dt$$

where $H_0 = 1$, $\sigma = 0.15$, and A was chosen so that the minimum thickness of the ice was 0.35. This integral is performed using Gauss-Legendre quadrature, and derivatives of H are readily obtained by taking derivatives of the Gaussian kernel above. The incident plane wave was chosen with wavenumber to be the same as the previous example, $k = 0.11$. When the incident wave reaches the groove, it excites a trapped mode that resonates throughout the spiral. These types of “waveguide” phenomena for surface waves are a rich area for future numerical investigations.

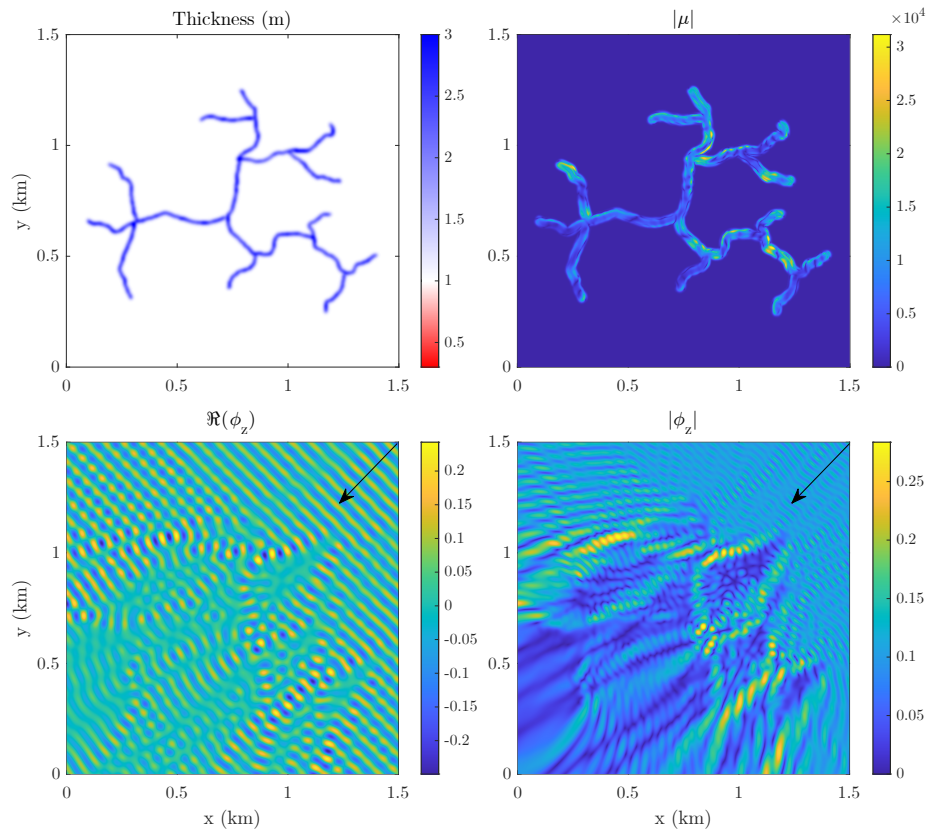


Figure 7: Wave scattering by a system of ridges. Top left: thickness profile. Top right: magnitude of the solution to the integral equation. Bottom left: Real part of the vertical velocity. Bottom right: magnitude of the vertical velocity. Black arrows indicate direction of incident field.

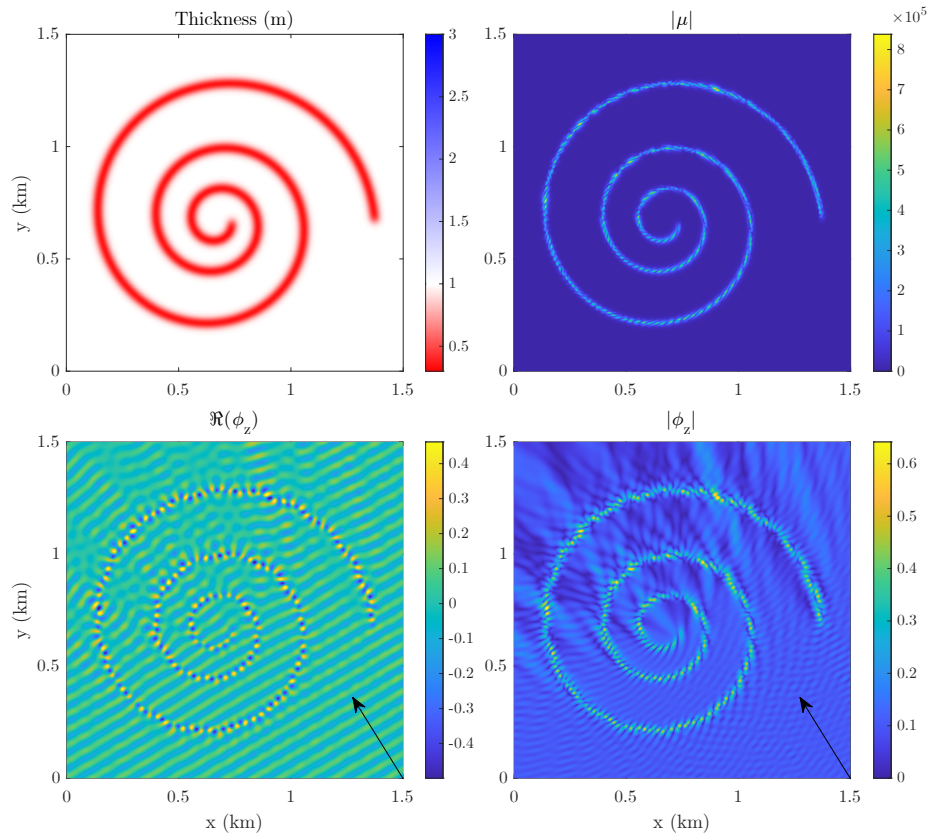


Figure 8: A spiral waveguide, with the same wavenumber as in the previous example (fig. 7). Top left: thickness profile. Top right: magnitude of the solution to the integral equation. Bottom left: Real part of the vertical velocity. Bottom right: magnitude of the vertical velocity. Black arrows indicate direction of incident field.

8 Conclusion

In this work, we develop a novel integral equation representation for the variable thickness problem in the modeling of flexural-gravity waves. The resulting integral equation is second-kind and its solution is compactly supported on the region of varying thickness. We prove well-posedness of the integral equation, i.e., that solutions exist for data in appropriate function spaces and that the solutions are unique and depend continuously on the data. To solve the integral equation numerically, we apply high-order accurate quadrature and solve the resulting linear system using an iterative algorithm with an FFT-accelerated matrix-vector product. The effectiveness and scalability of the method is demonstrated by solving several geometrically complex flexural-gravity scattering problems, inspired by applications in glaciology, that feature detailed branching patterns, Bragg scattering, multiple scattering, and trapped modes.

There are several extensions of this work that are of natural interest to applications in glaciology. These include polynyas (holes in the ice), ice floes of finite extent, and shore-fast ice. In these cases, the equations will need to be augmented with appropriate boundary conditions in some instances, and new Green's functions developed in others. Additionally, we have required that the coefficients α , β , and γ are smooth but this assumption can be weakened. In particular, one can augment the system with additional constraints which enforce continuity of the solution and its derivatives across lines where α is not differentiable. For a detailed discussion on how this is done in two dimensions, see [81]. We also note that the present method should extend easily to the case in which the depth of the fluid is finite but constant, via a standard *method of images* type approach. Though the form of the Green's function will change, much of the analysis, discretization, and solution should remain the same, *mutatis mutandis*. Such methods may be important for seismic imaging and passive sea-ice monitoring [70].

In this paper, a simple FFT-accelerated iterative solver was used. However, for more singular problems, e.g. problems in which the contrast ratio of α is high, many iterations may be required. For such nearly-singular problems, modern *fast direct* solvers can be easily adapted and extended to solve the discretized system. Such methods have the added benefit that, after an initial factorization step, it is relatively cheap to solve the system for many right-hand sides, which is particularly useful in optimization and inverse problems.

9 Code availability

The examples from this paper may be found at <https://github.com/peter-nekrasov/flex-plus-water>.

10 Acknowledgments

The authors would like to thank Douglas MacAyeal, Mary Silber, Anand Oza, Bowei Wu, Tristan Goodwill, and Michael Siegel for many useful discussions. P. Nekrasov would like to acknowledge the support of the National Science Foundation (NSF) under Grant No. 2332479. J.G. Hoskins and M. Rachh would like to thank the American Institute of Mathematics and, in particular, John Fry for hosting them on Bock Cay during the SQuaREs program, where parts of this work were completed. The Flatiron Institute is a division of the Simons Foundation.

References

- [1] Milton Abramowitz and Irene A Stegun. *Handbook of mathematical functions with formulas, graphs, and mathematical tables*, volume 55. US Government printing office, 1948.
- [2] H. Ammari, H. Kang, and H. Lee. *Layer Potential Techniques in Spectral Analysis*. AMS, 2009.
- [3] IV Andronov. The passage of a bending wave through an inhomogeneity in an absolutely rigid rib backing an elastic plate. *Journal of Mathematical Sciences*, 83:175–179, 1997.
- [4] IV Andronov and BP Belinskii. On acoustic boundary-contact problems for a vertically stratified medium bounded from above by a plate with concentrated inhomogeneities. *Journal of Applied Mathematics and Mechanics*, 54(3):366–371, 1990.
- [5] Matthew G. Asplin, Ryan Galley, David G. Barber, and Simon Prinsenber. Fracture of summer perennial sea ice by ocean swell as a result of Arctic storms. *Journal of Geophysical Research: Oceans*, 117(C6), 2012.
- [6] Guillaume Bal, Jeremy Hoskins, Solomon Quinn, and Manas Rachh. Integral formulation of Dirac singular waveguides, 2023.
- [7] Guillaume Bal, Jeremy Hoskins, Solomon Quinn, and Manas Rachh. Integral formulation of Klein–Gordon singular waveguides. *Communications on Pure and Applied Mathematics*, 78(2):323–365, 2025.
- [8] NJ Balmforth and RV Craster. Ocean waves and ice sheets. *Journal of Fluid Mechanics*, 395:89–124, 1999.
- [9] Murray D. Barrett and Vernon A. Squire. Ice-coupled wave propagation across an abrupt change in ice rigidity, density, or thickness. *Journal of Geophysical Research: Oceans*, 101(C9):20825–20832, 1996.

- [10] LG Bennetts, NRT Biggs, and D Porter. A multi-mode approximation to wave scattering by ice sheets of varying thickness. *Journal of Fluid Mechanics*, 579:413–443, 2007.
- [11] Luke G Bennetts, Nicholas RT Biggs, and David Porter. Wave scattering by an axisymmetric ice floe of varying thickness. *IMA journal of applied mathematics*, 74(2):273–295, 2009.
- [12] James Bremer, Zydrunas Gimbutas, and Vladimir Rokhlin. A Nonlinear Optimization Procedure for Generalized Gaussian Quadratures. *SIAM Journal on Scientific Computing*, 32(4):1761–1788, 2010.
- [13] Peter D Bromirski, Zhao Chen, Ralph A Stephen, Peter Gerstoft, D Arcas, Anja Diez, Richard C Aster, Douglas A Wiens, and Andrew Nyblade. Tsunami and infragravity waves impacting Antarctic ice shelves. *Journal of Geophysical Research: Oceans*, 122(7):5786–5801, 2017.
- [14] Peter D Bromirski and Ralph A Stephen. Response of the Ross Ice Shelf, Antarctica, to ocean gravity-wave forcing. *Annals of Glaciology*, 53(60):163–172, 2012.
- [15] Kelly M Brunt, Emile A Okal, and Douglas R MacAYEAL. Antarctic ice-shelf calving triggered by the Honshu (Japan) earthquake and tsunami, March 2011. *Journal of Glaciology*, 57(205):785–788, 2011.
- [16] Bas Buchner. An evaluation and extension of the shallow draft diffraction theory. In *ISOPE International Ocean and Polar Engineering Conference*, pages ISOPE–I. ISOPE, 1993.
- [17] LM Cathles IV, Emile A Okal, and Douglas R MacAyeal. Seismic observations of sea swell on the floating Ross Ice Shelf, Antarctica. *Journal of Geophysical Research: Earth Surface*, 114(F2), 2009.
- [18] A Chakrabarti. On the solution of the problem of scattering of surface-water waves by the edge of an ice cover. *Proceedings of the Royal Society of London. Series A: Mathematical, Physical and Engineering Sciences*, 456(1997):1087–1099, 2000.
- [19] Konstantinos Christakos, George Lavidas, Zhen Gao, and Jan-Victor Björkqvist. Long-term assessment of wave conditions and wave energy resource in the Arctic Ocean. *Renewable Energy*, 220:119678, 2024.
- [20] Hyuck Chung and Colin Fox. Calculation of wave-ice interaction using the Wiener-Hopf technique. *New Zealand J. Math*, 31(1):1–18, 2002.
- [21] Hyuck Chung and Colin Fox. Propagation of flexural waves at the interface between floating plates. In *ISOPE International Ocean and Polar Engineering Conference*, pages ISOPE–I. ISOPE, 2002.

- [22] Hyuck Chung and CM Linton. Reflection and transmission of waves across a gap between two semi-infinite elastic plates on water. *Quarterly Journal of Mechanics and Applied Mathematics*, 58(1):1–15, 2005.
- [23] Ian F Collins and IR McCrae. Creep buckling of ice shelves and the formation of pressure rollers. *Journal of glaciology*, 31(109):242–252, 1985.
- [24] Amir Darabi, Ahmad Zareei, Mohammad-Reza Alam, and Michael J Leamy. Broadband bending of flexural waves: acoustic shapes and patterns. *Scientific reports*, 8(1):1–7, 2018.
- [25] M De Corato and V Garbin. Capillary interactions between dynamically forced particles adsorbed at a planar interface and on a bubble. *Journal of fluid mechanics*, 847:71–92, 2018.
- [26] Anne-Sophie Bonnet-Ben Dhia, Luiz M. Faria, and Carlos Pérez-Arancibia. A Complex-Scaled Boundary Integral Equation for Time-Harmonic Water Waves. *SIAM Journal on Applied Mathematics*, 84(4):1532–1556, 2024.
- [27] *NIST Digital Library of Mathematical Functions*. <https://dlmf.nist.gov/>, Release 1.2.1 of 2024-06-15, 2024. F. W. J. Olver, A. B. Olde Daalhuis, D. W. Lozier, B. I. Schneider, R. F. Boisvert, C. W. Clark, B. R. Miller, B. V. Saunders, H. S. Cohl, and M. A. McClain, eds.
- [28] Ran Duan and Vladimir Rokhlin. High-order quadratures for the solution of scattering problems in two dimensions. *Journal of Computational Physics*, 228(6):2152–2174, 2009.
- [29] Charles L. Epstein, Leslie Greengard, Jeremy Hoskins, Shidong Jiang, and Manas Rachh. Coordinate complexification for the Helmholtz equation with Dirichlet boundary conditions in a perturbed half-space, 2024.
- [30] DV Evans and R Porter. Wave scattering by narrow cracks in ice sheets floating on water of finite depth. *Journal of fluid Mechanics*, 484:143–165, 2003.
- [31] Lawrence C Evans. *Partial differential equations*, volume 19. American Mathematical Society, 1998.
- [32] Colin Fox and Hyuck Chung. Green’s function for forcing of a thin floating plate. Technical report, Department of Mathematics, The University of Auckland, New Zealand, 1999.
- [33] Colin Fox and Vernon A. Squire. On the oblique reflexion and transmission of ocean waves at shore fast sea ice. *Philosophical Transactions of the Royal Society of London. Series A: Physical and Engineering Sciences*, 347(1682):185–218, 1994.
- [34] I.T.S. Gohberg and E.I. Sigal. Operator extension of the logarithmic residue theorem and Rouché’s theorem. *Mat. Sb. (N.S.)*, 84:607–642, 1971.

- [35] Oscar Gonzalez and Jun Li. A Convergence Theorem for a Class of Nyström Methods for Weakly Singular Integral Equations on Surfaces in \mathbb{R}^3 . *Mathematics of Computation*, 84(292):675–714, 2015.
- [36] Abinand Gopal and Per-Gunnar Martinsson. An accelerated, high-order accurate direct solver for the Lippmann–Schwinger equation for acoustic scattering in the plane. *Advances in Computational Mathematics*, 48(4):42, 2022.
- [37] Michael R Gorman. Plate wave acoustic emission. *The Journal of the Acoustical Society of America*, 90(1):358–364, 1991.
- [38] Izrail Solomonovich Gradshteyn and Iosif Moiseevich Ryzhik. *Table of integrals, series, and products*. Academic press, 2014.
- [39] WR Graham. Boundary layer induced noise in aircraft, Part I: The flat plate model. *Journal of Sound and Vibration*, 192(1):101–120, 1996.
- [40] AJ Hermans. The ray method for the deflection of a floating flexible platform in short waves. *Journal of Fluids and Structures*, 17(4):593–602, 2003.
- [41] WD Hibler III, WF Weeks, and SJ Mock. Statistical aspects of sea-ice ridge distributions. *Journal of Geophysical Research*, 77(30):5954–5970, 1972.
- [42] Anna E Hogg, Lin Gilbert, Andrew Shepherd, Alan S Muir, and Malcolm McMillan. Extending the record of Antarctic ice shelf thickness change, from 1992 to 2017. *Advances in Space Research*, 68(2):724–731, 2021.
- [43] Jeremy Hoskins, Manas Rachh, and Bowei Wu. On quadrature for singular integral operators with complex symmetric quadratic forms. *Applied and Computational Harmonic Analysis*, 2025.
- [44] Kevin Jose, Neil Ferguson, and Atul Bhaskar. Branched flows of flexural waves in non-uniform elastic plates. *Communications Physics*, 5(1):152, 2022.
- [45] Kevin Jose, Neil Ferguson, and Atul Bhaskar. Branched flows of flexural elastic waves in non-uniform cylindrical shells. *Plos one*, 18(5):e0286420, 2023.
- [46] AL Kohout, MJM Williams, Takenobu Toyota, Jan Lieser, and J Hutchings. In situ observations of wave-induced sea ice breakup. *Deep Sea Research Part II: Topical Studies in Oceanography*, 131:22–27, 2016.
- [47] Alison L Kohout, MJM Williams, SM Dean, and MH Meylan. Storm-induced sea-ice breakup and the implications for ice extent. *Nature*, 509(7502):604–607, 2014.
- [48] OP Kouzov. Diffraction of a plane hydroacoustic wave on the boundary of two elastic plates. *Journal of Applied Mathematics and Mechanics*, 27(3):806–815, 1963.

- [49] R. Kress. *Linear Integral Equations*. Applied Mathematical Sciences, Springer, 2014.
- [50] L.D. Landau and E.M. Lifshitz. *Theory of Elasticity: Course of Theoretical Physics*, volume 7. Pergamon Press, 1970.
- [51] Jack C Landy, Geoffrey J Dawson, Michel Tsamados, Mitchell Bushuk, Julianne C Stroeve, Stephen EL Howell, Thomas Krumpfen, David G Babb, Alexander S Komarov, Harry DBS Heorton, et al. A year-round satellite sea-ice thickness record from CryoSat-2. *Nature*, 609(7927):517–522, 2022.
- [52] Bernard Laulagnet. Sound radiation by a simply supported un baffled plate. *The Journal of the Acoustical Society of America*, 103(5):2451–2462, 1998.
- [53] Pei Li, Xuebing Chen, Xiaoming Zhou, Gengkai Hu, and Ping Xiang. Acoustic cloak constructed with thin-plate metamaterials. *International Journal of Smart and Nano Materials*, 6(1):73–83, 2015.
- [54] Wangtao Lu, Ya Yan Lu, and Jianliang Qian. Perfectly Matched Layer Boundary Integral Equation Method for Wave Scattering in a Layered Medium. *SIAM Journal on Applied Mathematics*, 78(1):246–265, 2018.
- [55] J. Ma, V. Rokhlin, and S. Wandzura. Generalized Gaussian Quadrature Rules for Systems of Arbitrary Functions. *SIAM Journal on Numerical Analysis*, 33(3):971–996, 1996.
- [56] AV Marchenko. Natural vibrations of a hummock ridge in an elastic ice sheet floating on the surface of an infinitely deep fluid. *Fluid dynamics*, 30(6):887–893, 1995.
- [57] AV Marchenko and KI Voliak. Surface wave propagation in shallow water beneath an inhomogeneous ice cover. *Journal of physical oceanography*, 27(8):1602–1613, 1997.
- [58] Michael H Meylan, Luke G Bennetts, JEM Mosig, WE Rogers, MJ Doble, and Malte A Peter. Dispersion relations, power laws, and energy loss for waves in the marginal ice zone. *Journal of Geophysical Research: Oceans*, 123(5):3322–3335, 2018.
- [59] Michael H. Meylan, Muhammad Ilyas, Bishnu P. Lamichhane, and Luke G. Bennetts. Swell-induced flexural vibrations of a thickening ice shelf over a shoaling seabed. *Proceedings of the Royal Society A: Mathematical, Physical and Engineering Sciences*, 477(2254):20210173, 2021.
- [60] John W. Miles. On the Aerodynamic Instability of Thin Panels. *Journal of the Aeronautical Sciences*, 23(8):771–780, 1956.
- [61] Peter Nekrasov and Douglas R. MacAyeal. Ocean wave blocking by periodic surface rolls fortifies Arctic ice shelves. *Journal of Glaciology*, page 1–11, 2023.

- [62] Peter Nekrasov, Tim Su, Travis Askham, and Jeremy G. Hoskins. Boundary Integral Formulations for Flexural Wave Scattering in Thin Plates, 2024.
- [63] Anand U Oza, Giuseppe Pucci, Ian Ho, and Daniel M Harris. Theoretical modeling of capillary surfer interactions on a vibrating fluid bath. *Physical Review Fluids*, 8(11):114001, 2023.
- [64] T.K. Papathanasiou and K.A. Belibassakis. A nonconforming hydroelastic triangle for ice shelf modal analysis. *Journal of Fluids and Structures*, 91:102741, 2019.
- [65] D Porter and R Porter. Approximations to wave scattering by an ice sheet of variable thickness over undulating bed topography. *Journal of Fluid Mechanics*, 509:145–179, 2004.
- [66] Richard Porter and DV Evans. Scattering of flexural waves by multiple narrow cracks in ice sheets floating on water. *Wave Motion*, 43(5):425–443, 2006.
- [67] M. Eric Reissner. Remark on the Theory of Bending of Plates of Variable Thickness. *Journal of Mathematics and Physics*, 16(1-4):43–45, 1937.
- [68] T Sahoo, Tsz Leung Yip, and Allen T Chwang. Scattering of surface waves by a semi-infinite floating elastic plate. *Physics of Fluids*, 13(11):3215–3222, 2001.
- [69] O. V. Sergienko. Behavior of flexural gravity waves on ice shelves: Application to the Ross Ice Shelf. *Journal of Geophysical Research: Oceans*, 122(8):6147–6164, 2017.
- [70] Robert A Shuchman, Clifford L Rufenach, and Ola M Johannessen. Extraction of marginal ice zone thickness using gravity wave imagery. *Journal of Geophysical Research: Oceans*, 99(C1):901–918, 1994.
- [71] Vernon A Squire. Of ocean waves and sea-ice revisited. *Cold Regions Science and Technology*, 49(2):110–133, 2007.
- [72] Vernon A Squire and Tony W Dixon. An analytic model for wave propagation across a crack in an ice sheet. *International Journal of Offshore and Polar Engineering*, 10(03), 2000.
- [73] Vernon A Squire and Tony W Dixon. How a region of cracked sea ice affects ice-coupled wave propagation. *Annals of Glaciology*, 33:327–332, 2001.
- [74] Vernon A Squire and Tony W Dixon. On modelling an iceberg embedded in shore-fast sea ice. *Journal of engineering mathematics*, 40:211–226, 2001.
- [75] Michael Eugene Taylor. *Partial differential equations. 1, Basic theory*. Springer, 1996.

- [76] NJ Teder, LG Bennetts, PA Reid, and RA Massom. Sea ice-free corridors for large swell to reach Antarctic ice shelves. *Environmental Research Letters*, 17(4):045026, 2022.
- [77] Gareth L Vaughan and Vernon A Squire. Scattering of ice-coupled waves by variable sea-ice terrain. *Annals of Glaciology*, 44:88–94, 2006.
- [78] Peter Wadhams, Vernon A. Squire, Dougal J. Goodman, Andrew M. Cowan, and Stuart C. Moore. The attenuation rates of ocean waves in the marginal ice zone. *Journal of Geophysical Research: Oceans*, 93(C6):6799–6818, 1988.
- [79] Catherine C. Walker, Joanna D. Millstein, Bertie W. J. Miles, Sue Cook, Alexander D. Fraser, Andreas Colliander, Sidharth Misra, Luke D. Trusel, Susheel Adusumilli, Chancellor Roberts, and Helen A. Fricker. Multi-decadal collapse of East Antarctica’s Conger–Glenzer Ice Shelf. *Nature Geoscience*, 17(12):1240–1248, Dec 2024.
- [80] WF Weeks and A Assur. *The mechanical properties of sea ice*, volume 2. US Army Materiel Command Cold Regions Research & Engineering Laboratory, 1967.
- [81] Timothy D Williams and Vernon A Squire. Oblique scattering of plane flexural–gravity waves by heterogeneities in sea–ice. *Proceedings of the Royal Society of London. Series A: Mathematical, Physical and Engineering Sciences*, 460(2052):3469–3497, 2004.
- [82] Bawei Wu and Per-Gunnar Martinsson. Corrected trapezoidal rules for boundary integral equations in three dimensions. *Numerische Mathematik*, 149:1025–1071, 2021.
- [83] Bawei Wu and Per-Gunnar Martinsson. Zeta correction: a new approach to constructing corrected trapezoidal quadrature rules for singular integral operators. *Advances in Computational Mathematics*, 47(3):45, 2021.
- [84] Bawei Wu and Per-Gunnar Martinsson. A Unified Trapezoidal Quadrature Method for Singular and Hypersingular Boundary Integral Operators on Curved Surfaces. *SIAM Journal on Numerical Analysis*, 61(5):2182–2208, 2023.
- [85] Ahmad Zareei and Mohammad-Reza Alam. Broadband cloaking of flexural waves. *Physical Review E*, 95(6):063002, 2017.

A Derivation of the Green’s function

By the translation invariance of (3.4), we can compute $G_S(\mathbf{r}, \mathbf{r}') = G_S(\mathbf{r} - \mathbf{r}', 0)$. Let $\hat{\sigma}(\xi)$ be the Fourier transform of $G_S(\mathbf{r}, 0)$. Taking a Fourier transform of

(3.4), we obtain

$$\left[(\alpha_0 |\xi|^4 - \beta_0) + \frac{\gamma}{|\xi|} \right] \hat{\sigma}(\xi) = 2.$$

Thus,

$$\hat{\sigma}(\xi) = \frac{2|\xi|}{\alpha_0 |\xi|^5 - \beta_0 |\xi| + \gamma}.$$

A.1 No repeated roots

Let ρ_1, \dots, ρ_5 be the roots of $p(z) = \alpha_0 z^5 - \beta_0 z + \gamma$ and let e_1, \dots, e_5 be defined as in (3.7). For now, we will assume that the roots are distinct as assumed in Lemma 3.1 and Theorem 3.1. We discuss appropriate modifications for treating repeated roots in Appendix A.2.

We perform a partial fraction expansion, obtaining

$$\hat{\sigma}(\xi) = 2|\xi| \sum_{j=1}^5 \frac{e_j}{|\xi| - \rho_j}.$$

Recalling the moment relations (3.8), $\hat{\sigma}$ can be re-expressed as

$$\hat{\sigma}(\xi) = 2 \sum_{j=1}^5 \frac{e_j \rho_j}{|\xi| - \rho_j}.$$

Taking an inverse Fourier transform, we obtain

$$G_S(\mathbf{r}, 0) = \frac{1}{\pi} \sum_{j=1}^5 e_j \rho_j \int_0^\infty \rho J_0(\rho r) \frac{1}{\rho - \rho_j} d\rho,$$

where $r = |\mathbf{r}|$. Rearranging, we see that

$$G_S(\mathbf{r}, 0) = \frac{1}{\pi} \sum_{j=1}^5 e_j \rho_j \int_0^\infty J_0(\rho r) d\rho + \frac{1}{\pi} \sum_{j=1}^5 e_j \rho_j^2 \int_0^\infty J_0(\rho r) \frac{1}{\rho - \rho_j} d\rho.$$

The moment relations (3.8) imply that the first term is zero.

Let $\chi \in \mathbb{C}$ be given with $\arg(\chi) \neq 0$. From [38, §6.562] we have the formula

$$\int_0^\infty J_0(\rho r) \frac{1}{\rho - \chi} d\rho = \frac{\pi}{2} \mathbf{K}_0(-\chi r)$$

where \mathbf{K}_0 is the standard Struve function. This formula covers most of the terms.

By Lemma 3.1, ρ_1 is the only root with zero argument. In this case, we determine the appropriate value for the limit by the limiting absorption principle. If $\rho_1(\beta)$ is the root of $\alpha z^5 - \beta z + \gamma$ continued from the root ρ_1 corresponding to $\beta = \beta_0$, then it is straightforward to show that

$$\left. \frac{\partial \rho_1(\beta)}{\partial \beta} \right|_{\beta=\beta_0} = \frac{\rho_1}{5\alpha\rho_1 - \beta_0} = \frac{\rho_1}{p'(\rho_1)} > 0.$$

Thus, for $\beta = \beta_0 + i\epsilon$, we have $\rho_1(\beta) \rightarrow \rho_1$ approaches from the upper half plane as $\epsilon \rightarrow 0^+$.

The function \mathbf{K}_0 has a branch cut on the negative real axis. In particular, $\mathbf{K}_0(z) = \mathbf{H}_0(z) - Y_0(z)$, where \mathbf{H}_0 is an analytic Struve function and Y_0 captures the branch cut. By convention, the value of Y_0 on the negative real axis is the limit of the principle branch from the upper half plane. We have also that $Y_0(ze^{m\pi i}) = Y_0(z) + 2imJ_0(z)$. After some re-arranging and applying standard identities, we obtain

$$\lim_{\epsilon \rightarrow 0^+} \mathbf{K}_0(-\rho_1(\beta_0 + i\epsilon)r) = -\mathbf{K}_0(\rho_1 r) + 2iH_0^{(1)}(\rho_1 r).$$

This recovers the formula (3.10).

Let $\hat{\sigma}_\phi$ be the Fourier transform of $G_\phi(\mathbf{r}, 0)$. By the definition of G_ϕ , (3.5), we have that

$$\hat{\sigma}_\phi(\xi) = \frac{\hat{\sigma}(\xi)}{2|\xi|} = \frac{1}{\alpha_0|\xi|^5 - \beta_0|\xi| + \gamma} = \sum_{j=1}^5 \frac{e_j}{|\xi| - \rho_j}.$$

Taking an inverse Fourier transform, we obtain

$$\begin{aligned} G_\phi(\mathbf{r}, 0) &= \frac{1}{2\pi} \sum_{j=1}^5 e_j \int_0^\infty \rho J_0(\rho r) \frac{1}{\rho - \rho_j} d\rho \\ &= \frac{1}{2\pi} \sum_{j=1}^5 e_j \int_0^\infty J_0(\rho r) d\rho + \frac{1}{2\pi} \sum_{j=1}^5 e_j \rho_j \int_0^\infty J_0(\rho r) \frac{1}{\rho - \rho_j} d\rho. \end{aligned}$$

Again, the moment relations and the Struve function integral identity applied above result in the formula (3.12).

Remark A.1. *The integral that defines G_ϕ in terms of G_S , i.e. (3.5), is absolutely convergent for $\epsilon \neq 0$ but only conditionally convergent for $\epsilon = 0$; c.f. Proposition 4.1. Observe that the limiting absorption approach is consistent with the principal value definition of the integral, as in (3.2), i.e. the formula (3.5) relating G_ϕ and G_S indeed holds.*

Remark A.2. *The above treats the physically meaningful case, $\gamma < 0$. For the non-physical case, $\gamma > 0$, the polynomial $p(z) = \alpha_0 z^5 - \beta_0 z + \gamma$ can have two positive roots for real β_0 . Because the derivative is positive at the larger of these roots and negative at the other, the dependence of the roots on β_0 takes opposite sign. One then finds that, when applying a limiting absorption principle, the roots approach the real axis from opposite sides. This has the amusing effect that there are two Hankel function terms in the limiting Green's function, one that is outgoing and one that is incoming.*

A.2 Repeated roots

In the case that $p(z) = \alpha_0 z^5 - \beta_0 z + \gamma$ has repeated roots, the procedure can be modified appropriately. Suppose that the roots are ρ_1, \dots, ρ_5 where $\rho_4 = \rho_5$ and ρ_1, \dots, ρ_3 are distinct. Then, we have a partial fraction decomposition

$$\frac{1}{\alpha_0 z^5 - \beta_0 z + \gamma} = \sum_{j=1}^4 \frac{e_j}{z - \rho_j} + \frac{\tilde{e}_4}{(z - \rho_4)^2}.$$

The coefficients e_1, \dots, e_4 are defined by residues as before, i.e. $e_j = \text{Res}_{z=\rho_j} 1/p(z)$ for $j = 1, \dots, 4$. The remaining coefficient can be found by the formula

$$\tilde{e}_4 = \text{Res}_{z=\rho_4} \frac{z - \rho_4}{p(z)}.$$

Similar moment relations can also be found by residue calculus. We have

$$\sum_{j=1}^4 e_j \rho_j^q + q \tilde{e}_4 \rho_4^{q-1} = 0 \text{ for } q \in \{0, 1, 2, 3\}, \quad \sum_{j=1}^4 e_j \rho_j^4 + 4 \tilde{e}_4 \rho_4^3 = \frac{1}{\alpha_0}.$$

We also have

$$\frac{2z}{\alpha_0 z^5 - \beta_0 z + \gamma} = 2 \sum_{j=1}^4 \frac{e_j \rho_j}{z - \rho_j} + 2 \frac{\tilde{e}_4}{z - \rho_4} + 2 \frac{\tilde{e}_4 \rho_4}{(z - \rho_4)^2}$$

A similar construction to the case with distinct roots gives

$$\begin{aligned} G_S(\mathbf{r}, 0) &= \frac{1}{\pi} \sum_{j=1}^4 e_j \rho_j \int_0^\infty \rho J_0(\rho r) \frac{1}{\rho - \rho_j} d\rho + \frac{1}{\pi} \tilde{e}_4 \int_0^\infty \rho J_0(\rho r) \frac{1}{\rho - \rho_4} d\rho \\ &\quad + \frac{1}{\pi} \tilde{e}_4 \rho_4 \int_0^\infty \rho J_0(\rho r) \frac{1}{(\rho - \rho_4)^2} d\rho, \end{aligned}$$

Rearranging, we see that

$$\begin{aligned} G_S(\mathbf{r}, 0) &= \frac{1}{\pi} \left(\sum_{j=1}^4 e_j \rho_j + \tilde{e}_4 \right) \int_0^\infty J_0(\rho r) d\rho + \frac{1}{\pi} \sum_{j=1}^3 e_j \rho_j^2 \int_0^\infty J_0(\rho r) \frac{1}{\rho - \rho_j} d\rho \\ &\quad + \frac{1}{\pi} (e_4 \rho_4^2 + 2 \tilde{e}_4 \rho_4) \int_0^\infty J_0(\rho r) \frac{1}{\rho - \rho_4} d\rho + \frac{1}{\pi} \tilde{e}_4 \rho_4^2 \int_0^\infty J_0(\rho r) \frac{1}{(\rho - \rho_4)^2} d\rho. \end{aligned}$$

Applying the same identities as before, we obtain

$$G_S(\mathbf{r}, 0) = \frac{1}{2}e_1\rho_1^2 \left[-\mathbf{K}_0(\rho_1 r) + 2iH_0^{(1)}(\rho_1 r) \right] + \frac{1}{2} \sum_{j=2}^3 e_j \rho_j^2 \mathbf{K}_0(-\rho_j r) \\ + \frac{1}{2} (e_4 \rho_4^2 + 2\tilde{e}_4 \rho_4) \mathbf{K}_0(-\rho_4 r) + \frac{1}{2} \tilde{e}_4 \rho_4^2 \left. \frac{\partial}{\partial \rho} \mathbf{K}_0(-\rho r) \right|_{\rho=\rho_4},$$

or more explicitly

$$G_S(\mathbf{r}, 0) = \frac{1}{2}e_1\rho_1^2 \left[-\mathbf{K}_0(\rho_1 r) + 2iH_0^{(1)}(\rho_1 r) \right] + \frac{1}{2} \sum_{j=2}^3 e_j \rho_j^2 \mathbf{K}_0(-\rho_j r) \\ + \frac{1}{2} (e_4 \rho_4^2 + 2\tilde{e}_4 \rho_4) \mathbf{K}_0(-\rho_4 r) + \frac{1}{2} \tilde{e}_4 \rho_4^2 \left(-\frac{2}{\pi} + \mathbf{K}_1(-\rho_4 r) \right) r.$$

We conclude with the following proposition, which characterizes the analyticity of G_S in the parameter β , independent of the presence of multiple roots.

Proposition A.1. *For fixed $\alpha_0 > 0$ and $\gamma < 0$ the Green's function G_S defined in (3.4) can be analytically continued as a function of β_0 from $\Im(\beta_0) > 0$ to an open neighborhood of $\Im(\beta_0) \geq 0$.*

Proof. It is elementary to show that for $\alpha_0 > 0$ and $\gamma < 0$ fixed, the polynomial $\alpha_0 z^5 - \beta_0 z + \gamma$ has exactly one positive real root for any $\beta \in \mathbb{R}$, which we denote by $\rho(\beta_0)$. It follows that, in a neighborhood, this root, being isolated, is an analytic function of β_0 . Thus, in the vicinity of any $\beta_* \in \mathbb{R}$ we can perform the partial fraction decomposition, splitting $z \alpha_0 (\alpha_0 z^5 - \beta_0 z + \gamma)^{-1}$ into

$$\frac{1}{4\rho^4 - \frac{\gamma}{\alpha_0\rho}} \frac{\rho}{z - \rho} - \frac{\rho}{4\rho^4 - \frac{\gamma}{\alpha_0\rho}} \frac{z^3 + 2\rho z^2 + 3\rho^2 z + \frac{\gamma}{\alpha_0\rho^2}}{z^4 + \rho z^3 + \rho^2 z^2 + \rho^3 z - \frac{\gamma}{\alpha_0\rho}}$$

where the root ρ is an analytic function of β_0 near β_* . Moreover, the denominator of the second term is bounded away from zero for all $z \in \mathbb{R}^+ \cup \{0\}$, and $\rho(\beta_*) > 0$. To proceed further, we can rewrite this as

$$\frac{2\rho^2}{4\rho^4 - \frac{\gamma}{\alpha_0\rho}} \left[\frac{1}{z^2 - \rho^2} - \frac{1}{z^2 + \rho^2} \right] \\ - \frac{\rho}{4\rho^4 - \frac{\gamma}{\alpha_0\rho}} \left[\frac{z^3 + 2\rho z^2 + 3\rho^2 z + \frac{\gamma}{\alpha_0\rho^2}}{z^4 + \rho z^3 + \rho^2 z^2 + \rho^3 z - \frac{\gamma}{\alpha_0\rho}} - \frac{1}{z + \rho} - \frac{2\rho}{z^2 + \rho^2} \right]. \quad (\text{A.1})$$

We label these terms as T_1 and T_2 , respectively.

We note that by the construction of the partial fraction decomposition, the second term, T_2 , is $O(z^{-4})$ as $z \rightarrow \infty$ uniformly for β in a neighborhood of β_* . Replacing z in the previous expression by $\sqrt{\xi} \cdot \xi$ and taking the inverse Fourier transform, the above calculations show that the inverse Fourier transform of

the first term, T_1 , gives rise to an analytic function of β_0 , $\Im\beta_0 > 0$, which can be analytically continued to $\Im\beta_0 \leq 0$. For $\mathbf{r} \neq \mathbf{0}$, performing a contour deformation so that $\arg \sqrt{\xi} \cdot \bar{\xi} \equiv \theta_0 < 0$, it is clear that the contribution of the second term is analytic in β near β_* . Finally, straightforward asymptotic analysis shows that near $\mathbf{r} = 0$, the inverse Fourier transform of T_2 looks like $\sigma(\beta_0)r^2 \log(r) + \psi(r, \beta_0)$, where σ is analytic in β_0 , ψ is three times differentiable in r and analytic in β_0 .

For $\Im\beta_* > 0$ we can establish analyticity in β near β_* by directly by taking the inverse Fourier transform of $|\xi|/(\alpha_0|\xi|^5 - \beta_0|\xi| + \gamma)$. Similarly, for $\Im\beta_* < 0$ we can perform the same analysis, combined with the identity $\mathbf{K}_0(ze^{2\pi i}) = \mathbf{K}_0(z) - 4iJ_0(z)$, to continue onto the next sheet.

It follows immediately that G_S is analytic in β_0 in an open neighborhood of $\Im\beta_0 \geq 0$. Similar reasoning can be applied to the derivatives of G_S up to order 3. It follows immediately that the integral operators in (3.14) are analytic in this region. \square

B Numerical evaluation of Struve and related functions

Though Struve functions arise in a wide variety of applications, there appear to be relatively few accurate and efficient algorithms for their evaluation. In this section we briefly describe a numerical method for their computation. For ease of exposition, we define the related functions \mathbf{R}_n defined by

$$\mathbf{R}_n(z) := J_n(z) + i\mathbf{H}_n(z).$$

Here we focus on \mathbf{R}_0 and \mathbf{R}_1 . In principle, together with the three-term recurrence,

$$\mathbf{R}_{\nu-1}(z) + \mathbf{R}_{\nu+1}(z) = \frac{2\nu}{z}\mathbf{R}_\nu(z) + \frac{i\left(\frac{z}{2}\right)^\nu}{\sqrt{\pi}\Gamma\left(\nu + \frac{3}{2}\right)}$$

this can be extended to the computation of higher-order Struve functions. Derivatives of \mathbf{R}_ν can similarly be calculated using the relation

$$\mathbf{R}_{\nu-1}(z) - \mathbf{R}_{\nu+1}(z) = 2\mathbf{R}'_\nu(z) - \frac{i\left(\frac{z}{2}\right)^\nu}{\sqrt{\pi}\Gamma\left(\nu + \frac{3}{2}\right)}.$$

We consider two separate cases, depending on the magnitude of z . For small z we use generalized Gaussian quadrature together with an integral representation of \mathbf{R}_n . For large z we use an asymptotic expansion.

In the first case, we use the following Lemma which follows immediately from [1].

Lemma B.1. *Let $\mathbf{R}_n(z)$ be the function defined by $\mathbf{R}_n(z) = J_n(z) + i\mathbf{H}_n(z)$. Then, for any $z \in \mathbb{C}$, and $n \geq 0$, \mathbf{R}_n has the integral representation*

$$\mathbf{R}_n(z) = \frac{2\left(\frac{z}{2}\right)^n}{\sqrt{\pi}\Gamma\left(n + \frac{1}{2}\right)} \int_0^1 (1-t^2)^{n-1/2} e^{izt} dt.$$

Next, we have the following result which provides an upper bound on the number of quadrature nodes required to numerically compute the above integrals for z in the upper halfplane with non-negative imaginary part.

Proposition B.1. *For $z \in \mathbb{C}$ with $\Im z \geq 0$, consider the function $f_z : [0, 1] \rightarrow \mathbb{C}$ defined by*

$$f_z(t) = \frac{(1-t^2)^n}{\sqrt{1+t}} e^{izt}.$$

For any $\epsilon > 0$ there exists an $m < C(n+|z|+\log \epsilon^{-1})$ together with a polynomial $p \in P_m$ such that $\|p - f_z\|_\infty < \epsilon$. Moreover, if $|z| < R$ then m can be chosen independent of $|z|$.

In light of the above proposition, given a tolerance ϵ , and letting $m = m(n, \epsilon)$, then it follows that there exists an m point quadrature rule which integrates

$$I_{n,z} = \int_0^1 (1-t^2)^{n-1/2} e^{izt} dt$$

with an error bounded by 2ϵ for any $z \in \mathbb{C}$, with $|z| < R$, and $\Im z \geq 0$.

The above analysis guarantees slow growth in the size of the quadrature rule as a function of the z cutoff, accuracy requirements, and order. In principle, it can be used constructively to produce suitable quadratures. In our calculations we fix $\epsilon = 10^{-12}$ and $R = 95$. Using a generalized Gaussian quadrature method [55, 12], we obtain a 38 point quadrature rule to approximate $I_{n,z}$ for $n = 0, 1$. In order to be able to compute $\mathbf{R}_{0,1}$ everywhere in the upper halfplane we require an algorithm for computing values for $|z| \geq 95$. Here we use the asymptotic series. The cut-off of $|z| = 95$ is chosen to guarantee that the asymptotic series gives at least an absolute error of 10^{-12} . In particular, we have the expansion [1]

$$\mathbf{K}_\nu(z) \sim \frac{1}{\pi} \sum_{n=0}^{\infty} \frac{\Gamma(n+1/2) \left(\frac{z}{2}\right)^{\nu-2k-1}}{\Gamma(\nu+1/2-k)}.$$

This, coupled with the identity

$$\mathbf{R}_\nu(z) = \mathbf{K}_\nu(z) - H_\nu(z),$$

gives an asymptotic expansion for \mathbf{R}_ν in terms of the above expansion and the standard asymptotic expansions for the Hankel function H_ν [1].

C Derivatives of the Green's function

In this section, we compute the derivatives of the Green's function (3.10). Recall that we have the following recurrence relations for the Hankel function of the first kind:

$$\begin{aligned} H_0^{(1)'}(z) &= -H_1^{(1)}(z), \\ H_1^{(1)'}(z) &= H_0^{(1)}(z) - \frac{1}{z} H_1^{(1)}(z), \end{aligned}$$

As well as the following recurrence relations for the Struve function of the second kind:

$$\begin{aligned}\mathbf{K}'_0(z) &= \frac{2}{\pi} - \mathbf{K}_1(z) \\ \mathbf{K}'_1(z) &= \mathbf{K}_0(z) - \frac{1}{z}\mathbf{K}_1(z)\end{aligned}$$

Taking derivatives of (3.10) with respect to the target variable \mathbf{r} , we obtain:

$$\begin{aligned}\nabla_{\mathbf{r}} G_S(\mathbf{r}, \mathbf{r}') &= \frac{\mathbf{r} - \mathbf{r}'}{|\mathbf{r} - \mathbf{r}'|} M_1(\mathbf{r}, \mathbf{r}') \\ H[G_S](\mathbf{r}, \mathbf{r}') &= \frac{-1}{|\mathbf{r} - \mathbf{r}'|^3} \begin{pmatrix} (x-x')^2 - (y-y')^2 & 2(x-x')(y-y') \\ 2(x-x')(y-y') & (y-y')^2 - (x-x')^2 \end{pmatrix} M_1(\mathbf{r}, \mathbf{r}') \\ &\quad + \frac{1}{|\mathbf{r} - \mathbf{r}'|^2} \begin{pmatrix} (x-x')^2 & (x-x')(y-y') \\ (x-x')(y-y') & (y-y')^2 \end{pmatrix} M_2(\mathbf{r}, \mathbf{r}') \\ \Delta_{\mathbf{r}} G_S(\mathbf{r}, \mathbf{r}') &= M_2(\mathbf{r}, \mathbf{r}') \\ \nabla_{\mathbf{r}} \Delta_{\mathbf{r}} G_S(\mathbf{r}, \mathbf{r}') &= -\frac{\mathbf{r} - \mathbf{r}'}{|\mathbf{r} - \mathbf{r}'|} M_3(\mathbf{r}, \mathbf{r}')\end{aligned}$$

where $H[G_S]$ is the Hessian of G_S and the functions M_1, M_2, M_3 are given by:

$$\begin{aligned}M_1(\mathbf{r}, \mathbf{r}') &= \frac{1}{2}e_1\rho_1^3[\mathbf{K}_1(\rho_1|\mathbf{r} - \mathbf{r}'|) - 2iH_1^{(1)}(\rho_1|\mathbf{r} - \mathbf{r}'|)] + \frac{1}{2}\sum_{j=2}^5 e_j\rho_j^3\mathbf{K}_1(-\rho_j|\mathbf{r} - \mathbf{r}'|) \\ M_2(\mathbf{r}, \mathbf{r}') &= \frac{1}{2}e_1\rho_1^4[\mathbf{K}_0(\rho_1|\mathbf{r} - \mathbf{r}'|) - 2iH_0^{(1)}(\rho_1|\mathbf{r} - \mathbf{r}'|)] - \frac{1}{2}\sum_{j=2}^5 e_j\rho_j^4\mathbf{K}_0(-\rho_j|\mathbf{r} - \mathbf{r}'|) \\ M_3(\mathbf{r}, \mathbf{r}') &= \frac{1}{2}e_1\rho_1^5[\mathbf{K}_1(\rho_1|\mathbf{r} - \mathbf{r}'|) - 2iH_1^{(1)}(\rho_1|\mathbf{r} - \mathbf{r}'|)] + \frac{1}{2}\sum_{j=2}^5 e_j\rho_j^5\mathbf{K}_1(-\rho_j|\mathbf{r} - \mathbf{r}'|)\end{aligned}$$

D Proof of convergence

Given a second kind integral equation with a weakly-singular integral kernel with smooth enough coefficients and a suitable quadrature rule, it is natural to expect the resulting Nyström scheme to converge at the same order as the quadrature rule. In this section, we prove this for a class of integral equations which includes (3.14), discretized using a corrected trapezoid rule. The proof follows standard lines, see [49, 35]; we include it here for completeness. The crux is to show that, for fine enough grids, the discretized linear system is invertible, with a bound on the inverse independent of the grid size. This is established in Corollary D.1.

Given a region Ω containing the support of f , let $\Omega_0 = [-L, L] \times [-L, L]$ be such $\Omega \subset \Omega_0$ and that the boundary of Ω is a distance $d > 0$ from the

boundary of Ω_0 . We consider the case in which we are given an integral operator $K : C(\Omega_0) \rightarrow C(\Omega_0)$, with kernel

$$k(\mathbf{x}, \mathbf{y}) = \sum_{j=1}^m \beta_j(\mathbf{x}) w_j(\mathbf{x} - \mathbf{y}).$$

We further assume that the functions β_j are smooth and compactly supported in Ω , and that each w_j satisfies estimates of the kind

$$|w(\mathbf{x})| \leq \frac{w_*}{|\mathbf{x}|}, \quad |\nabla w(\mathbf{x})| \leq \frac{w_d}{|\mathbf{x}|^2}$$

for all $|x| \leq \text{diam } \Omega_0$. Let $\beta_* := \max_j \|\beta_j\|_\infty$ and $\beta_d := \max_j \|\nabla \beta_j\|_\infty$.

In the discretization of our problem we consider equispaced grids with spacing h . In the following, we assume that $h = 2L/(2N + 1)$ for some large enough integer $N > 0$. Let $\mathbf{x}_i^h = \mathbf{i}h$, where $\mathbf{i} = (i_1, i_2)$, $i_1, i_2 \in -N, -N + 1, \dots, N$ denote the locations of the discretization nodes. Given the plethora of indices in the following, we suppress the dependence of h on N .

For each h , each point \mathbf{x}_i^h and each j , we construct a quadrature for w_j which is of the form $\omega_{\mathbf{i}, \mathbf{i}'}^{j, h} = w_j(h(\mathbf{i} - \mathbf{i}')) h^2$ if $\mathbf{i} - \mathbf{i}' \notin \mathcal{C}$ and $\omega_{\mathbf{i}, \mathbf{i}'}^{j, h} = \alpha_{\mathbf{i} - \mathbf{i}'}^j(h)$ if $\mathbf{i} - \mathbf{i}' \in \mathcal{C}$. Here \mathcal{C} is a fixed finite set (the stencil) independent of h and $\alpha_{\mathbf{i}}^j(h)$ are quadrature corrections which may depend on h but satisfy the bound $|\alpha_{\mathbf{i}}^j(h)| \leq \alpha_* h$. We further require $(0, 0) \in \mathcal{C}$. Furthermore, we assume that the stencil and corrections are chosen so that for some integer $p > 0$, and any smooth function μ on Ω_0

$$\sup_{\mathbf{x}_i^h \in \Omega} \left| \sum_{\mathbf{i}'} \omega_{\mathbf{i}, \mathbf{i}'}^{j, h} \mu(\mathbf{x}_{\mathbf{i}'}^h) - \int_{\Omega_0} w_j(\mathbf{x}_i^h - \mathbf{y}) \mu(\mathbf{y}) \, d\mathbf{y} \right| < Ah^p \quad (\text{D.1})$$

for some constant A depending on μ .

The discretization of K is then given by

$$\underline{K}^h[\mu](\mathbf{x}_i^h) = \sum_{\mathbf{i}'} \sum_{j=1}^m \beta_j(\mathbf{x}_i^h) \omega_{\mathbf{i}, \mathbf{i}'}^{j, h} \mu(\mathbf{x}_{\mathbf{i}'}^h).$$

We can extend this to a continuous function on Ω_0 by setting $\underline{K}^h[\mu](\mathbf{x})$ to be the continuous piecewise linear interpolant agreeing with $\underline{K}^h[\mu](\mathbf{x}_i^h)$ at each \mathbf{x}_i^h , and 0 on $\partial\Omega_0$. The interpolant is chosen to be linear on each triangle formed by splitting one of the grid squares in half along the bottom left to top right diagonal. For ease of exposition we set $L_i^h(\mathbf{x})$ to be the coefficient of $\mu(\mathbf{x}_i^h)$ in $\underline{K}^h[\mu](\mathbf{x})$.

As noted above, the main analytical result we will establish is that the finite-rank operators $\{\underline{K}^h\}$ and the corresponding fully-discrete operators for such a quadrature rule are invertible for sufficiently small h . The aim of this appendix is to prove the following three results.

Theorem D.1. *Suppose that $I + K$ is invertible on $C(\Omega_0)$. In the notation above, $(I + \underline{K}^h)^{-1}$ exists and $\|(I + \underline{K}^h)^{-1}\|_{C(\Omega_0)}$ is bounded by a constant independent of h , for h sufficiently small.*

The following corollary is an immediate consequence of the previous theorem.

Corollary D.1. *Under the same conditions as Theorem D.1, the matrix $\mathbf{I} + \mathbf{K}^h$, where $K_{ij}^h = L_j^h(\mathbf{x}_i^h)$, is invertible and the ℓ^∞ norm condition number of the family of matrices satisfies a uniform bound for h sufficiently small.*

Theorem D.2. *Suppose $f \in C_c^\infty(\Omega)$, extended to 0 in $\Omega_0 \setminus \Omega$. Suppose further that μ solves $(I + K)\mu = f$, and that μ^h solves $(I + K^h)\mu^h = f$. Then there exists a constant C such that*

$$\max_i |\mu(\mathbf{x}_i) - \mu^h(\mathbf{x}_i)| \leq Ch^p$$

for h sufficiently small.

We prove Theorem D.1 using a mild extension of the strategy employed in [49, Ch. 10–12]. The idea of the proof is to apply the following result about the pointwise convergence of collectively compact families of operators, which is a consequence of the Banach-Steinhaus theorem or uniform boundedness principle.

Lemma D.1. [49, Thm. 10.12 and Cor. 10.11] *Let X be a Banach space and let $A : X \rightarrow X$ be a compact operator such that $I + A$ is injective on X . Suppose that $H > 0$ and that $\{A^h\}$ for $0 < h \leq H$ is a collectively compact set of operators such that $A^h \mu \rightarrow A\mu$ as $h \rightarrow 0$ for all $\mu \in X$. Then, $(I + A^h)^{-1}$ exists and $\|(I + A^h)^{-1}\|_X$ is bounded by a constant independent of h , for h sufficiently small.*

To apply this result, we need to establish the compactness of the original operator K , the collective compactness of the family of finite-rank operators $\{\underline{K}^h\}$, and the pointwise convergence of these same operators. That K is compact follows immediately from standard results, see [49, Thm. 2.22] for example, together with the behavior of the kernels near the diagonal.

In order to establish the collective compactness of the family $\{\underline{K}^h\}$, we require the following two lemmas, whose proof we defer to the end of the appendix.

Lemma D.2. *With L_i^h as defined above, if $h < d$ then there exists a constant C_1 , independent of h , such that*

$$\sum_{i'} |L_{i'}^h(\mathbf{x})| \leq C_1$$

for all $x \in \Omega_0$. In particular,

$$\sup_{0 < h < d} \|\underline{K}^h\|_\infty < C_1.$$

Lemma D.3. *With L_i^h defined as above, then for each $\eta \in (0, 1)$, there exists a constant C_2 , depending on η but not on h , such that*

$$\sum_{i'} |L_{i'}^h(\mathbf{x}) - L_{i'}^h(\mathbf{y})| \leq C_2 \|\mathbf{x} - \mathbf{y}\|^\eta$$

for all $0 < h < \max\{d, 1\}$ and all $x, y \in \Omega_0$. In particular, for any bounded set $U \subset C(\Omega_0)$, the set

$$\{\underline{K}^h \mu : \mu \in U \text{ and } 0 < h < d\}$$

is equicontinuous.

From the two previous lemmas, the collective compactness follows immediately.

Lemma D.4. *In the notation above, the operators $\{\underline{K}^h\}$, for $0 < h < d$, are collectively compact.*

Proof. By the Arzelà-Ascoli theorem, collective compactness is equivalent to the boundedness and equicontinuity of sets of the form $\{\underline{K}^h \mu\}$ where the μ come from a bounded subset of $C(\Omega_0)$ and $0 < h < d$. These are established in Lemmas D.2 and D.3, respectively, in appendix D. \square

We also require the following Lemma, which gives the pointwise convergence of the operators \underline{K}^h to K .

Lemma D.5. *For any $\sigma \in C(\Omega_0)$,*

$$\lim_{h \rightarrow 0^+} \sup_{\mathbf{x} \in \Omega_0} |\underline{K}^h[\mu](\mathbf{x}) - K[\mu](\mathbf{x})| = 0.$$

Proof. It suffices to show that the result holds for smooth functions. The result then follows by combining (D.1) for $\mathbf{x} \in \Omega$, the fact that both $\underline{K}^h[\mu]$ and $K[\mu]$ are identitically 0 for $\mathbf{x} \in \Omega_0 \setminus \Omega$, the uniform continuity of $K[\mu]$, and the piecewise linear nature of the \underline{K}^h , together with the existence of a bound on $\sup_{0 < h < d} \|\underline{K}^h\|_\infty, \|K\|_\infty$. \square

We now proceed with the proof of Theorem D.1.

Proof of Theorem D.1, and Corollary D.1. Applying Lemmas D.4 and D.5, we have that the family $\{\underline{K}^h\}$ and the operator K satisfy the conditions of Lemma D.1 on the space $C(\Omega_0)$, establishing Theorem D.1.

To prove Corollary D.1, we make the observation that the semi-discrete operators $I + \underline{K}^h$ map piecewise linear interpolants over the grid points to piecewise linear interpolants over the grid points. Let h be sufficiently small that the operators $I + \underline{K}^h$ are invertible and the norms $\|(I + \underline{K}^h)^{-1}\|_{C(\Omega_0)}$ satisfy a uniform bound. Suppose, by contradiction, that the discrete operator $\mathbf{I} + \mathbf{K}^h$ has a non-zero null vector. Then, the piecewise linear interpolant of the values specified by this null vector gets mapped to the zero function by $I + \underline{K}^h$, a contradiction. Likewise, the correspondence of the ℓ^∞ norm of the interpolation values

and the $C(\Omega_0)$ norm of the interpolant for piecewise linear interpolants over the grid points implies that $\|(\mathbf{I} + \mathbf{K}^h)^{-1}\|_\infty$ is bounded uniformly for sufficiently small h . \square

Proof of Theorem D.2. Corollary 4.3 along with the assumptions imply that $\mu \in C_c^\infty(\Omega_0)$. Applying the estimate (D.1) to μ , we get that $\sup_{\mathbf{i}} |K_h[\mu](\mathbf{x}_i) - K[\mu](\mathbf{x}_i)| \leq Ch^p$ for some constant C and h sufficiently small. Letting $\delta_{\mathbf{i}} = \mu(\mathbf{x}_i^h) - \mu^h(\mathbf{x}_i^h)$, we note that the difference satisfies the linear system $(\mathbf{I} + \mathbf{K}^h)\boldsymbol{\delta} = \mathbf{g}$, where $g_{\mathbf{i}} = (K_h - K)[\mu](\mathbf{x}_i)$, and $\boldsymbol{\delta}$ and \mathbf{g} are the vectors with components $\delta_{\mathbf{i}}$, and $g_{\mathbf{i}}$. The result then follows from Corollary D.1. \square

We conclude with the proofs of the two lemmas, Lemma D.2 and Lemma D.3. In the following we use C , and its various decorations, to denote arbitrary constants independent of h , with values that can change from line to line. In our analysis we will make frequent use of the following bounds. The proof is straightforward and omitted.

Lemma D.6. *Let $p \in \mathbb{R}_+$ and $M \in \mathbb{Z}_+$, be given. Then there exist constants $c > 0$ and $C < \infty$, depending on p but independent of M , such that*

$$c \int_{1/2}^M \frac{1}{r^{p-1}} dr \leq \sum_{1 \leq \|\mathbf{i}\|_\infty \leq M} \frac{1}{|\mathbf{i}|^p} \leq C \int_{1/2}^M \frac{1}{r^{p-1}} dr.$$

Moreover, there exists a constant \tilde{C} such that for any $1 \leq \rho_1 < \rho_2 < \infty$,

$$\sum_{\rho_1 \leq |\mathbf{i}| \leq \rho_2} \frac{1}{|\mathbf{i}|^p} \leq \tilde{C} \int_{\rho_1 - \frac{1}{\sqrt{2}}}^{\rho_2 + \frac{1}{\sqrt{2}}} \frac{1}{r^{p-1}} dr.$$

Proof of Lemma D.2. We first prove the inequality for $\mathbf{x} = \mathbf{x}_i^h$, the case of general \mathbf{x} following by linearity. Then,

$$\sum_{\mathbf{i}-\mathbf{i}' \notin \mathcal{C}} |L_{\mathbf{i}'}^h(\mathbf{x})| = \sum_{j=1}^m \sum_{\mathbf{i}-\mathbf{i}' \notin \mathcal{C}} |\beta_j(\mathbf{x}_i^h)| |w_j(h(\mathbf{i}-\mathbf{i}'))| h^2 \leq \beta_* m \sum_{\mathbf{i}-\mathbf{i}' \notin \mathcal{C}} w_* h^2 \frac{1}{h|\mathbf{i}-\mathbf{i}'|}.$$

Using the previous lemma, it follows that

$$\sum_{\mathbf{i}-\mathbf{i}' \notin \mathcal{C}} |L_{\mathbf{i}'}^h(\mathbf{x})| \leq \tilde{C} \text{diam } \Omega_0. \quad (\text{D.2})$$

A bound on the remaining portion, the sum over $\mathbf{i}-\mathbf{i}' \in \mathcal{C}$, can be obtained from the bounds on the $\alpha_{\mathbf{i}}^h$,

$$\sum_{\mathbf{i}-\mathbf{i}' \in \mathcal{C}} |L_{\mathbf{i}'}^h(\mathbf{x}_i^h)| \leq |C| \beta_* m \alpha_* h. \quad (\text{D.3})$$

Combining (D.2) and (D.3) yields the desired result. \square

For ease of exposition, let $\mathcal{C}^h(\mathbf{x})$ denote the indices of the grid points with corrections for the point \mathbf{x} with grid size h . We note that $|\mathcal{C}^h(\mathbf{x})| \leq 4|\mathcal{C}|$. We now prove Lemma D.3.

Proof of Lemma D.3. From the previous lemma, it suffices to establish this for $\|\mathbf{x} - \mathbf{y}\| < 1$. We begin by observing that for any grid point \mathbf{x}_ℓ^h ,

$$L_{\mathbf{i}'}^h(\mathbf{x}_\ell^h) = \sum_{j=1}^m \beta_j(\mathbf{x}_\ell^h) w_j(h(\ell - \mathbf{i}')) h^2 + \sum_{j=1}^m \beta_j(\mathbf{x}_\ell^h) \tilde{\alpha}_{\ell - \mathbf{i}'}^j(h) =: T_{\mathbf{i}'}^h(\mathbf{x}_\ell^h) + S_{\mathbf{i}'}^h(\mathbf{x}_\ell^h)$$

where $\tilde{\alpha}_{\mathbf{i}}^j = \alpha_{\mathbf{i}}^j - w_j(h\mathbf{i})h^2$ if $\mathbf{i} \in \mathcal{C}$, $\mathbf{i} \neq (0,0)$, $\tilde{\alpha}_{(0,0)}^j = \alpha_{(0,0)}^j$, and $\tilde{\alpha}_{\mathbf{i}}^j = 0$ for $\mathbf{i} \notin \mathcal{C}$. We note that the assumptions on the kernels w_j guarantee that $|\tilde{\alpha}_{\mathbf{i}}^j| \leq \tilde{\alpha}_* h$ for some constant $\tilde{\alpha}_*$ independent of h . By linearity, if we use the same interpolation rule for $T_{\mathbf{i}'}^h$ and $S_{\mathbf{i}'}^h$ as for L^h , we can define $T_{\mathbf{i}'}^h, S_{\mathbf{i}'}^h \in C(\Omega)$, with $L_{\mathbf{i}'}^h(\mathbf{x}) = T_{\mathbf{i}'}^h(\mathbf{x}) + S_{\mathbf{i}'}^h(\mathbf{x})$.

We first consider $E = \sum_{\mathbf{i}'} |S_{\mathbf{i}'}^h(\mathbf{x}) - S_{\mathbf{i}'}^h(\mathbf{y})|$ and note from the definition of $S_{\mathbf{i}}^h$ that

$$E = \sum_{\mathbf{i}'} |\chi_{\mathbf{i}' \in \mathcal{C}^h(\mathbf{x})} S_{\mathbf{i}'}^h(\mathbf{x}) - \chi_{\mathbf{i}' \in \mathcal{C}^h(\mathbf{y})} S_{\mathbf{i}'}^h(\mathbf{y})|.$$

For any point $\mathbf{x} \in \Omega_0$ we observe that by construction there exist coefficients $q_{\mathbf{i}}(x)$ such that

$$\chi_{\mathbf{i}' \in \mathcal{C}^h(\mathbf{x})} S_{\mathbf{i}'}^h(\mathbf{x}) = \sum_{\mathbf{i}} q_{\mathbf{i}}(\mathbf{x}) \chi_{\mathbf{i}' \in \mathcal{C}^h(\mathbf{x}_{\mathbf{i}}^h)} S_{\mathbf{i}'}^h(\mathbf{x}_{\mathbf{i}}^h) = \sum_{\mathbf{i}} q_{\mathbf{i}}(x) \chi_{\mathbf{i} - \mathbf{i}' \in \mathcal{C}} S_{\mathbf{i}'}^h(\mathbf{x}_{\mathbf{i}}^h).$$

Moreover, for all \mathbf{i} , $q_{\mathbf{i}}(\mathbf{x})$ is a Lipschitz function of \mathbf{x} with Lipschitz constant bounded by Q/h for some universal constant Q . Finally, $\sum_{\mathbf{i}} |q_{\mathbf{i}}(\mathbf{x})| = 1$, and for any $\mathbf{x} \in \Omega$, $q_{\mathbf{i}}(\mathbf{x})$ has at most 3 nonzero entries, thinking of it as a vector indexed by \mathbf{i} . Then,

$$E = \sum_{\mathbf{i}} |q_{\mathbf{i}}(\mathbf{x}) - q_{\mathbf{i}}(\mathbf{y})| \sum_{\mathbf{i}'} \chi_{\mathbf{i} - \mathbf{i}' \in \mathcal{C}} |S_{\mathbf{i}'}^h(\mathbf{x}_{\mathbf{i}}^h)|.$$

We next observe that for $\mathbf{i} - \mathbf{i}' \in \mathcal{C}$,

$$|S_{\mathbf{i}'}^h(\mathbf{x}_{\mathbf{i}}^h)| \leq \beta_* \sum_{j=1}^m |\tilde{\alpha}_{\mathbf{i} - \mathbf{i}'}^j(h)| \leq m \beta_* \tilde{\alpha}_* h.$$

Thus,

$$E \leq 6Q \tilde{\alpha}_* \beta_* m |\mathcal{C}| |\mathbf{x} - \mathbf{y}|.$$

Turning to $T_{\mathbf{i}'}^h$, we first consider the case in which \mathbf{x} and \mathbf{y} are grid points \mathbf{x}_ℓ^h and $\mathbf{x}_{\ell'}^h$, respectively. Next, we observe that from our assumptions,

$$|\nabla(\beta_j(\mathbf{x}) w_j)| \leq \frac{|\nabla \beta_j(\mathbf{x})| w_*}{|\mathbf{x}|} + \frac{|\beta_j(\mathbf{x})| w_d}{|\mathbf{x}|^2} \leq \frac{\tilde{C}}{|\mathbf{x}|^2}.$$

and, in particular,

$$|T_{\mathbf{i}'}^h(\mathbf{x}_\ell^h) - T_{\mathbf{i}'}^h(\mathbf{x}_{\ell'}^h)| \leq \tilde{C}h|\ell - \ell'| \sup_{t \in [0,1]} \frac{1}{|t\ell + (1-t)\ell' - \mathbf{i}'|^2}.$$

Set ℓ_* to be the nearest grid point to $(\ell + \ell')/2$. Then,

$$\sum_{|\mathbf{i}' - \ell_*| > h^{\eta-1}|\ell - \ell'|^{\eta+3}|\ell - \ell'|} |T_{\mathbf{i}'}^h(\mathbf{x}_\ell^h) - T_{\mathbf{i}'}^h(\mathbf{x}_{\ell'}^h)| \leq C'h \int_{h^{\eta-1}|\ell - \ell'|^\eta}^{2 \text{diam } \Omega_0 / h} \frac{1}{r} dr \leq C''h \log(h).$$

where the constants C' and C'' are independent of ℓ, ℓ' , and h . In the inner region, $|\mathbf{i}' - \ell_*| \leq h^{\eta-1}|\ell - \ell'|^{\eta+3}|\ell - \ell'|$ we use the bounds on the w_j directly, to obtain

$$\begin{aligned} \sum_{|\mathbf{i}' - \ell_*| \leq h^{\eta-1}|\ell - \ell'|^{\eta+3}|\ell - \ell'|} |T_{\mathbf{i}'}^h(\mathbf{x}) - T_{\mathbf{i}'}^h(\mathbf{y})| &\leq \sum_{|\mathbf{i}' - \ell_*| \leq h^{\eta-1}|\ell - \ell'|^{\eta+3}|\ell - \ell'|} |T_{\mathbf{i}'}^h(\mathbf{x})| + |T_{\mathbf{i}'}^h(\mathbf{y})| \\ &\leq 2C''''h \int_0^{h^{\eta-1}|\ell - \ell'|+5|\ell - \ell'|} 1 dr \\ &\leq C''''h^\eta |\ell - \ell'|^\eta = C''''|\mathbf{x}_\ell^h - \mathbf{x}_{\ell'}^h|^\eta. \end{aligned}$$

Combining this with the previous estimate for the outer region gives

$$\sum_{\mathbf{i}'} |T_{\mathbf{i}'}^h(\mathbf{x}_\ell^h) - T_{\mathbf{i}'}^h(\mathbf{x}_{\ell'}^h)| \leq C|\mathbf{x}_\ell^h - \mathbf{x}_{\ell'}^h|^\eta$$

for some constant C independent of h, ℓ , and ℓ' .

We now turn to the case of arbitrary \mathbf{x} and \mathbf{y} . From the above estimate, the difference between the sum at neighboring grid points is bounded by Ch^η , and hence, for \mathbf{x} and \mathbf{y} in the same triangle,

$$\sum_{\mathbf{i}'} |T_{\mathbf{i}'}^h(\mathbf{x}) - T_{\mathbf{i}'}^h(\mathbf{y})| \leq C'|\mathbf{x} - \mathbf{y}|h^{\eta-1} \leq C''|\mathbf{x} - \mathbf{y}|^\eta.$$

The first inequality above gives that $T_{\mathbf{i}'}^h$, viewed as a vector-valued function of \mathbf{x} equipped with the ℓ_1 norm, is Lipschitz, with Lipschitz constant bounded by $C'h^{\eta-1}$. If $|\mathbf{x} - \mathbf{y}| < 10h$ then it follows that

$$\sum_{\mathbf{i}'} |T_{\mathbf{i}'}^h(\mathbf{x}) - T_{\mathbf{i}'}^h(\mathbf{y})| \leq C'|\mathbf{x} - \mathbf{y}|h^{\eta-1} \leq C'|\mathbf{x} - \mathbf{y}|^{1-\eta+\eta}h^{\eta-1} \leq 10C'|\mathbf{x} - \mathbf{y}|^\eta.$$

Now suppose that $|\mathbf{x} - \mathbf{y}| > 10h$. Let \mathbf{x}_ℓ^h and $\mathbf{x}_{\ell'}^h$ be the closest grid points to \mathbf{x} and \mathbf{y} , respectively. Clearly, $|\mathbf{x} - \mathbf{y}| > 1/2(|\mathbf{x} - \mathbf{x}_\ell^h| + |\mathbf{x}_\ell^h - \mathbf{x}_{\ell'}^h| + |\mathbf{x}_{\ell'}^h - \mathbf{y}|)$. From the above inequalities it follows that

$$\begin{aligned} \sum_{\mathbf{i}'} |T_{\mathbf{i}'}^h(\mathbf{x}) - T_{\mathbf{i}'}^h(\mathbf{y})| &\leq C''(|\mathbf{x} - \mathbf{x}_\ell^h|^\eta + |\mathbf{x}_{\ell'}^h - \mathbf{y}|^\eta) + C|\mathbf{x}_\ell^h - \mathbf{x}_{\ell'}^h|^\eta \\ &\leq 3^{1-\eta}(C'' + C)(|\mathbf{x} - \mathbf{x}_\ell^h| + |\mathbf{y} - \mathbf{x}_{\ell'}^h| + |\mathbf{x}_\ell^h - \mathbf{x}_{\ell'}^h|)^\eta \\ &\leq 3^{1-\eta}2^\eta(C'' + C)|\mathbf{x} - \mathbf{y}|^\eta. \end{aligned}$$

where the second to last inequality follows from Hölder's inequality.

To conclude, combining the bounds on the differences of the S^h and T^h terms, we see that for all $|\mathbf{x} - \mathbf{y}| \leq 1$,

$$\sum_{i'} |L_{i'}^h(\mathbf{x}) - L_{i'}^h(\mathbf{y})| \leq C_* |\mathbf{x} - \mathbf{y}|^\eta$$

independent of h . The constant C_* does not depend on \mathbf{x}, \mathbf{y} , or h , though it does depend on η . \square